Photometry and Spectroscopy of GRB 030329 and Its Associated Supernova 2003dh: The First Two Months

T. Matheson[1], P. M. Garnavich[2], K. Z. Stanek[1], D. Bersier[1], S. T. Holland[2,3], K. Krisciunas[4,5], N. Caldwell[1], P. Berlind[6], J. S. Bloom[1], M. Bolte[7], A. Z. Bonanos[1], M. J. I. Brown[8], W. R. Brown[1], M. L. Calkins[6], P. Challis[1], R. Chornock[9], L. Echevarria[10], D. J. Eisenstein[11], M. E. Everett[12], A. V. Filippenko[9], K. Flint[13], R. J. Foley[9], D. L. Freedman[1], Mario Hamuy[14], P. Harding[15], N. P. Hathi[10], M. Hicken[1], C. Hoopes[16], C. Impey[11], B. T. Jannuzi[8], R. A. Jansen[10], S. Jha[9], J. Kaluzny[17], S. Kannappan[18], R. P. Kirshner[1], D. W. Latham[1], J. C. Lee[11], D. C. Leonard[19], W. Li[9], K. L. Luhman[1], P. Martini[14], H. Mathis[8], J. Maza[20], S. T. Megeath[1], L. R. Miller[8], D. Minniti[21], E. W. Olszewski[11], M. Papenkova[9], M. M. Phillips[4], B. Pindor[22], D. D. Sasselov[1], R. Schild[1], H. Schweiker[23], T. Spahr[1], J. Thomas-Osip[4], I. Thompson[14], D. Weisz[9], R. Windhorst[10], and D. Zaritsky[11]

[1]Harvard-Smithsonian Center for Astrophysics, 60 Garden Street, Cambridge, MA 02138

[2]Dept. of Physics, University of Notre Dame, 225 Nieuwland Science Hall, Notre Dame, IN 46556

[3]Current Address: Goddard Space Flight Center, Code 662.20, Greenbelt, MD, 20771-0003

[4]Carnegie Institution of Washington, Las Campanas Observatory, Casilla 601, La Serena, Chile

[5]Cerro Tololo Inter-American Observatory, Casilla 603, La Serena, Chile

[6]F. L. Whipple Observatory, 670 Mt. Hopkins Road, P.O. Box 97, Amado, AZ 85645

[7]University of California Observatories/Lick Observatory, University of California, Santa Cruz, Santa Cruz, CA 95064

[8]National Optical Astronomy Observatory, 950 North Cherry Ave., Tucson, AZ 85719

[9]University of California, Dept. of Astronomy, 601 Campbell Hall, Berkeley CA, 94720-3411

[10]Dept. of Physics and Astronomy, Arizona State University, Tempe, AZ 85287-1504

[11]Steward Observatory, University of Arizona, 933 N. Cherry Ave., Tucson, AZ 85718

[12]Planetary Sciences Institute, 620 N. Sixth Avenue, Tucson, Arizona 85705

[13]Carnegie Institution of Washington, DTM, 5241 Broad Branch Road, NW Washington, DC 20015

[14]Carnegie Observatories, 813 Santa Barbara Street, Pasadena, CA 91101

[15]Dept. of Astronomy, Case Western Reserve University, 10900 Euclid Avenue, Cleveland, OH 44106

[16]Dept. of Physics and Astronomy, Johns Hopkins University, 3400 N. Charles St., Baltimore, MD 21218

[17]Copernicus Astronomical Center, Bartycka 18, PL-00-716, Warsaw, Poland

[18]The University of Texas at Austin, McDonald Obs., 1 University Station C1402, Austin, TX 78712-0259

[19]Five College Astronomy Department, University of Massachusetts, Amherst, MA 01003-9305

[20]Universidad de Chile, Casilla 36-D, Santiago, Chile

[21]Pontificia Universidad Católica de Chile, Casilla 306, Santiago, 22, Chile

[22]Princeton University Observatory, Princeton, NJ 08544

[23]WIYN Consortium Inc., 950 N Cherry Ave., Tucson, AZ 85719

tmatheson@cfa.harvard.edu, pgarnavi@miranda.phys.nd.edu, kstanek@cfa.harvard.edu, dbersier@cfa.harvard.edu, sholland@milkyway.gsfc.nasa.gov, kevin@ctiosz.ctio.noao.edu, ncaldwell@cfa.harvard.edu, pberlind@cfa.harvard.edu, jbloom@cfa.harvard.edu, bolte@ucolick.org, abonanos@cfa.harvard.edu, mbrown@noao.edu, wbrown@cfa.harvard.edu, mcalkins@cfa.harvard.edu, pchallis@cfa.harvard.edu, chornock@astron.berkeley.edu, Luis.Echevarria@asu.edu, eisenste@as.arizona.edu, everett@psi.edu, alex@astron.berkeley.edu, flint@dtm.ciw.edu, rfoley@astron.berkeley.edu, dfreedman@cfa.harvard.edu, mhamuy@ociw.edu, harding@billabong.astr.cwru.edu, nphathi@asu.edu, mhicken@cfa.harvard.edu, choopes@pha.jhu.edu, impey@as.arizona.edu, jannuzi@noao.edu, Rolf.Jansen@asu.edu, saurabh@astron.berkeley.edu, jka@camk.edu.pl, sheila@astro.as.utexas.edu, rkirshner@cfa.harvard.edu, dlatham@cfa.harvard.edu, jlee@as.arizona.edu, leonard@nova.astro.umass.edu, weidong@astron.berkeley.edu, kluhman@cfa.harvard.edu, martini@ociw.edu, hmathis@noao.edu, jose@das.uchile.cl, tmegeath@cfa.harvard.edu, mmiller@noao.edu, dante@astro.puc.cl, edo@as.arizona.edu, marina@ugastro.berkeley.edu, mmp@lco.cl, pindor@astro.princeton.edu, dsasselov@cfa.harvard.edu, rschild@cfa.harvard.edu, heidis@noao.edu, tspahr@cfa.harvard.edu, jet@lco.cl, ian@ociw.edu, dweisz@uclink.berkeley.edu, Rogier.Windhorst@asu.edu, dzaritsky@as.arizona.edu

ABSTRACT

We present extensive optical and infrared photometry of the afterglow of gamma-ray burst (GRB) 030329 and its associated supernova (SN) 2003dh over the first two months after detection (2003 March 30-May 29 UT). Optical spectroscopy from a variety of telescopes is shown and, when combined with the photometry, allows an unambiguous separation between the afterglow and supernova contributions. The optical afterglow of the GRB is initially a power-law continuum but shows significant color variations during the first week that are unrelated to the presence of a supernova. The early afterglow light curve also shows deviations from the typical power-law decay. A supernova spectrum is first detectable ~ 7 days after the burst and dominates the light after ~ 11 days. The spectral evolution and the light curve are shown to closely resemble those of SN 1998bw, a peculiar Type Ic SN associated with GRB 980425, and the time of the supernova explosion is close to the observed time of the GRB. It is now clear that at least some GRBs arise from core-collapse SNe.

Subject headings: galaxies: distances and redshifts — gamma-rays: bursts — supernovae: general — supernovae: individual (SN 2003dh)

1. Introduction

The mechanism that produces gamma-ray bursts (GRBs) has been the subject of considerable speculation during the four decades since their discovery (see Mészáros 2002 for a recent review of the theories of GRBs). The discovery of optical afterglows (e.g., GRB 970228: Groot et al. 1997; van Paradijs et al. 1997) opened a new window on the field (see, e.g., van Paradijs, Kouveliotou, & Wijers 2000). Subsequent studies of other bursts yielded the redshifts of several GRBs (e.g., GRB 970508: Metzger et al. 1997), providing definitive evidence for their cosmological origin. Observations at other wavelengths, especially radio, have revealed many more details about the bursts (e.g., Berger et al. 2000; Frail et al. 2003).

Models that invoked supernovae (SNe) to explain GRBs were proposed from the very beginning (e.g., Colgate 1968; Woosley 1993; Woosley & MacFadyen 1999). There have been tantalizing observational clues that also pointed to SNe as a possible mechanism for producing GRBs. The most direct was GRB 980425: no traditional GRB optical afterglow was seen, but a supernova, SN 1998bw, was found in the error box of the GRB (Galama et al. 1998a). The SN was classified as a Type Ic (Patat & Piemonte 1998), but it was unusual, with high expansion velocities (Patat et al. 2001). Other SNe with high expansion velocities (and usually large luminosity as well) such as SN 1997ef and SN 2002ap are sometimes referred to as "hypernovae" (see, e.g., Iwamoto et al. 1998, 2000). GRB 980425 was also unusual in the sense that the isotropic energy of the burst was 10^{-3} to 10^{-4} times weaker than in classical cosmological GRBs (Woosley, Eastman, & Schmidt 1999), indicating that this was not a typical burst.

Indirect evidence also relates GRBs to SNe. Core-collapse SNe are associated with massive stars (e.g., Van Dyk, Hamuy, & Filippenko 1996) and GRBs also appear to be associated with massive stars, based on their location in their host galaxies (e.g., Bloom, Kulkarni, & Djorgovski 2002) and statistics of the types of galaxies that host GRBs (e.g., Hogg & Fruchter 1999). Chevalier & Li (2000) have shown that the afterglow properties of some GRBs are consistent with a shock moving into a stellar wind formed from a massive star.

The redshift of a typical GRB is $z \approx 1$, implying that a supernova component underlying an optical afterglow would be difficult to detect. At $z \approx 1$, even a bright core-collapse event would peak at $R > 23$ mag. Nevertheless, late-time deviations from the power-law decline typically observed for optical afterglows have been seen and these bumps in the light curves have been interpreted as evidence for supernovae (for a recent summary, see Bloom 2003). Perhaps the best evidence that classical, long-duration gamma-ray bursts are generated by core-collapse supernovae was provided by GRB 011121. It was at $z = 0.36$, so the supernova component would have been relatively bright. A bump in the light curve was observed both from the ground and with *HST* (Garnavich et al. 2003a; Bloom et al. 2002). The color changes in the light curve of GRB 011121 were also consistent with a supernova (designated SN 2001ke), but a spectrum obtained by Garnavich et al. (2003a) during the time that the bump was apparent did not show any features that could be definitively identified as originating from a supernova. The detection of a clear spectroscopic supernova signature was for the first time reported for the GRB 030329 by Matheson et al. (2003a, 2003b), Garnavich et al. (2003b, 2003c), Chornock et al. (2003), and Stanek et al. (2003a). Hjorth et al. (2003) also presented spectroscopic data obtained with the VLT. Their analysis produced results similar to those presented here. In addition, Kawabata et al. (2003) obtained a spectrum of SN 2003dh with the Subaru telescope. The properties of the afterglow light curve have also been described by Burenin et al. (2003), Uemura et al. (2003), and Price et al. (2003).

The extremely bright GRB 030329 was detected by the French Gamma Ray Telescope, the Wide Field X-Ray Monitor, and the Soft X-Ray Camera instruments aboard the *High Energy Transient Explorer II* at 11:37:14.67 (UT is used throughout this paper) on 2003 March 29 (Vanderspek et al. 2003). With a duration of more than 25 seconds, GRB 030329 is classified as a long-duration burst (Kouveliotou et al. 1993). Peterson & Price (2003) and Torii (2003) reported discovery of a bright ($R \approx 13$ mag), slowly fading optical transient (OT), located at $\alpha = 10^{\mathrm{h}}44^{\mathrm{m}}50\overset{\mathrm{s}}{.}0$, $\delta = +21°31'17\overset{''}{.}8$ (J2000.0), and identified this as the GRB optical afterglow. Due to the brightness of the afterglow, observations of the optical transient (OT) were extensive, making it most likely the best-observed afterglow so far.

From the moment the low redshift of 0.1685 for the GRB 030329 was announced (Greiner et al. 2003), we started organizing a campaign of spectroscopic and photometric follow-up of the afterglow and later the possible associated supernova. Stanek et al. (2003a) reported the first results of this campaign, namely a clear spectroscopic detection of a SN 1998bw-like supernova in the early spectra, designated SN 2003dh (Garnavich et al. 2003c). In this paper, we report on our extensive data taken for GRB 030329/SN 2003dh during the first two months after the burst.

2. The Photometric Data

The photometric data are listed in Table 1[24]. Much of our $UBVR_CI_C$ photometry was obtained with the F. L. Whipple Observatory (FLWO) 1.2-m telescope and the "4Shooter" CCD mosaic (Szentgyorgyi et al., in preparation) with four thinned, back-side illuminated,

[24]The analysis presented here supersedes our GCN Circulars by Martini et al. (2003), Garnavich et al. (2003d), Stanek, Martini & Garnavich (2003), Li et al. (2003a, b), Bersier et al. (2003b), and Stanek et al. (2003b).

AR-coated Loral 2048 × 2048 pixel CCDs. The camera has a pixel scale of $0.335''$ pixel^{-1} and a field of view of roughly $11.5'$ on a side for each chip. The data were taken in the 2×2 CCD binning mode. We continuously monitored the afterglow during the first night in all five bands, obtaining a total of 149 images. We also obtained multi-band data each night for the next 11 nights. We then closely followed the OT in the R band with only two gaps, when the Moon was very bright or close to the object and when the "4Shooter" was not on the telescope[25].

Extensive early $UBVRI$ data were also obtained using an Apogee AP7 CCD camera with the 0.76-m Katzman Automatic Imaging Telescope (KAIT; Li et al. 2000; Filippenko et al. 2001) at Lick Observatory. The Apogee camera has a back-illuminated SITe 512×512 pixel CCD chip, which with a scale of $0\farcs8$ pixel^{-1} yields a total field of view of $6'.7 \times 6'.7$. Thirteen $UBVRI$ sets were obtained during the first night, and three sets the next night (Li et al. 2003a).

Additional R-band images, including our earliest photometric data, were obtained using the Magellan telescopes at Las Campanas Observatory (LCO) with the LDSS2 imaging spectrograph (Mulchaey 2001) in its imaging mode, with a scale of $0\farcs378$ pixel^{-1}. We also obtained R-band data with the LCO Swope 1-m telescope equipped with the SITe#3 2048 × 3150 CCD camera, which with a scale of $0\farcs435$ pixel^{-1} yields a total field of view of $14'.8 \times 22'.8$. Also at LCO, we obtained BVI images with the du Pont 2.5-m telescope equipped with the TEK#5 2048 × 2048 pixel CCD camera, which with a scale of $0\farcs259$ pixel^{-1} yields a total field of view of $8'.85 \times 8'.85$.

In the B and R bands we obtained a significant number of images with the KPNO Mayall 4-m telescope equipped with the MOSAIC-1 wide-field camera. The prime focus Mosaic-1 camera (Muller et al. 1998) has eight CCDs covering its $36' \times 36'$ field of view. For the majority of the exposures, the telescope was pointed so that GRB 030329 and photometry reference objects were all placed on the second of the eight CCDs. The images were all processed through the reduction steps listed in version 7.01 of "The NOAO Deep Wide-Field Survey MOSAIC Data Reductions" guide through the application of a dome flat (Jannuzi et al. in preparation)[26]. The software used for the reductions is described by Valdes (2002). All of the software is part of the MSCRED software package (v4.7), which is part of IRAF[27].

---

[25]All photometry and spectroscopy presented in this paper are available through `anonymous ftp` on `cfa-ftp.harvard.edu`, in the directory `pub/kstanek/GRB030329`, and through the `WWW` at `http://cfa-www.harvard.edu/cfa/oir/Research/GRB/`.

[26]http://www.noao.edu/noao/noaodeep/ReductionOpt/frames.html

[27]IRAF is distributed by the National Optical Astronomy Observatory, which is operated by the Associa-

Additional late B-band data were obtained with the du Pont 2.5-m telescope. We also obtained late B-band data with the FLWO 1.2-m telescope.

The data were reduced by several of us using different photometry packages. We used DoPHOT (Schechter et al. 1993), DAOPHOT II (Stetson, 1987, 1992; Stetson & Harris 1988), and in some cases the image subtraction code ISIS (Alard & Lupton 1998; Alard 2000). We found excellent agreement among the various packages. Images were brought onto a common zero point using from 10 to >100 stars per image, depending on the filter and depth of the image. We used several field stars measured by Henden (2003) to obtain calibrated magnitudes.

In addition, a KAIT calibration of the GRB 030329 field was done on May 22 UT, 2003 by observing Landolt standard stars (Landolt 1992) at a large range of airmasses under photometric conditions. Aperture photometry was performed on these standard star frames in IRAF and then used to calibrate three local standard stars in the KAIT field of GRB 030329. Comparison of the KAIT and the Henden calibrations shows that they are consistent with each other (to within 0.03 mag). The KAIT data were in excellent agreement with the overlapping FLWO data, with the largest offset of only 0.03 mag in the V band. Such uniform data allow a great level of detail in analyzing the evolution of the OT.

In the infrared (IR), the OT was observed with the LCO Swope 1-m telescope IR camera equipped with Rockwell NICMOS3 HgCdTe 256×256 pixel array with $0\farcs6$ pixel^{-1} scale, yielding a $2'.5 \times 2'.5$ field of view (Persson et al. 1995). The data were obtained from 2003 April 2 to 10, using the J_s and H filters. Typically, three standard stars (Persson et al. 1998) were observed each night, one each at the beginning, middle, and end of the night. We assumed mean values of extinction appropriate at LCO: J_s (0.10 mag/airmass) and H (0.04 mag/airmass). For a comparison star near the GRB, with brightness comparable to the OT, this resulted in photometry with a scatter lower than 0.04 mag, indicating accurate and stable photometry for the whole run.

3. The Spectroscopic Data

Spectra of the OT associated with GRB 030329 were obtained over many nights with the 6.5-m MMT telescope, the 1.5-m Tillinghast telescope at the F. L. Whipple Observatory (FLWO), the Magellan 6.5-m Clay and Baade telescopes at LCO, the du Pont 2.5-m

tion of Universities for Research in Astronomy, Inc., under cooperative agreement with the National Science Foundation.

telescope at LCO, the Shane 3-m telescope at Lick Observatory, and the Keck I and II 10-m telescopes[28]. The majority of the data discussed herein are from the MMT. The spectrographs used were the Blue Channel (Schmidt et al. 1989) at MMT, FAST (Fabricant et al. 1998) at FLWO, LDSS2 (Mulchaey 2001) with Clay, the Boller & Chivens (Phillips et al. 2002) with Baade, the WFCCD (Weymann et al. 1999) with du Pont, the Kast Double Spectrograph (Miller & Stone 1993) at Lick, LRIS (Oke et al. 1995) with Keck I, and ESI (Sheinis et al. 2002) with Keck II. Standard CCD processing and spectrum extraction were accomplished with IRAF. Except for the April 24 ESI data, all spectra were optimally extracted (Horne 1986). The wavelength scale was established with low-order polynomial fits to calibration lamp spectra taken near the times of the OT exposures. Small-scale adjustments derived from night-sky lines in the OT frames were also applied. We employed our own routines in IDL to flux calibrate the spectra; spectrophotometric standards, along with other observational details, are listed in Table 2. We attempted to remove telluric lines using the well-exposed continua of the spectrophotometric standards (Wade & Horne 1988; Matheson et al. 2000).

The spectra were in general taken at or near the parallactic angle (Filippenko 1982) and at low airmass (with the obvious exception of observations from LCO). The relative fluxes are thus accurate to $\sim 5\%$ over the entire wavelength range. The Blue Channel, LDSS2, and Boller & Chivens spectrographs suffer from second-order contamination with the gratings used for these observations. Through careful cross-calibration with standard stars of different colors (and order-sorting filters with the Boller & Chivens), we believe that we have minimized the effects of the second-order light. For the few nights at the MMT when a broad range of standard stars of different colors was not available, we used the closest match from either the preceding or following night. Comparison with broad-band photometry indicates that the overall shape of the spectra is correct.

4. Early Photometry and Spectroscopy: Days 1-12

The transition between the afterglow and the supernova was gradual, so we define our "early" data based on our observations. We obtained spectroscopic data each of the 12 nights between March 30 and April 10. For each of these nights, we also obtained multi-band photometric data.

---

[28]The analysis presented here supersedes our GCN and IAU Circulars by Martini et al. (2003), Caldwell et al. (2003), Matheson et al. (2003a), Garnavich et al. (2003b), Matheson et al. (2003b), Garnavich et al. (2003c), and Chornock et al. (2003).

4.1. Early Photometry

We plot our GRB 030329 $UBVRIJH$ light curves in Figure 1. Within the first 24 hours, the light curve of the afterglow consisted of a broken power law typical of many well-observed bursts (Garnavich et al. 2003d). But the optical afterglow exhibited unusual behavior over the following week that has been analyzed in numerous GCNs (e.g., Li et al. 2003b, c). As it is clear that the afterglow cannot be well described with any semblance of a smooth function usually fitted to describe the OT evolution, we present and discuss here only our data. Such uniform data allow a great level of detail and confidence in analyzing the evolution of the GRB, including color changes, not usually possible when using non-homogeneous data compiled from the GCNs and the literature.

This is another clear example of an OT changing color as it fades. A color change was also seen in the OT of GRB 021004 (Matheson et al. 2003c; Bersier et al. 2003a). The color curves of the OT of GRB 030329 are plotted in Figure 2, in which the color changes are more readily apparent (see also Zeh, Klose, & Greiner 2003). These changes are discussed in more detail below when we describe the evolution of the spectral energy distribution (SED).

GRB 030329 is located at Galactic coordinates $l = 216\overset{\circ}{.}9867, b = 60\overset{\circ}{.}6997$. To remove the effects of the Galactic interstellar extinction we used the reddening map of Schlegel, Finkbeiner, & Davis (1998) which yields $E(B-V) = 0.025$ mag. This corresponds to expected values of Galactic extinction ranging from $A_H = 0.014$ to $A_U = 0.137$ mag, using the extinction corrections of Cardelli, Clayton, & Mathis (1989) and O'Donnell (1994) as prescribed in Schlegel et al. (1998).

We synthesized the $UBVRI$ spectrum for the first seven nights and $BVRI$ spectra for later nights from our data by using our best, most closely spaced measurements for all the nights (Figure 3). We converted the magnitudes to fluxes using the effective frequencies and normalizations of Fukugita et al. (1995). These conversions are accurate to better than 4%, so to account for the calibration errors we added a 4% error in quadrature to the statistical error in each flux measurement.

There are several evolutionary stages to be noticed in Figure 3. First, the SED gradually evolves between the first and the third night (see the dotted line in Figure 3), with the spectrum becoming steeper (redder). The spectral index, corrected for Galactic reddening of $E(B-V) = 0.025$ mag, changes from -0.71 the first night, through -0.89 the second night, to -0.97 the third night. Our early shallower slope agrees well with the -0.66 slope measured by Burenin et al. (2003) in their earlier data taken $6-11$ hours after the burst. Our data are also consistent with the dereddened spectral slope of -0.85 found using SDSS photometry coinciding with our second night data (Lee et al. 2003). Then, at $\Delta T = 4.65$ days

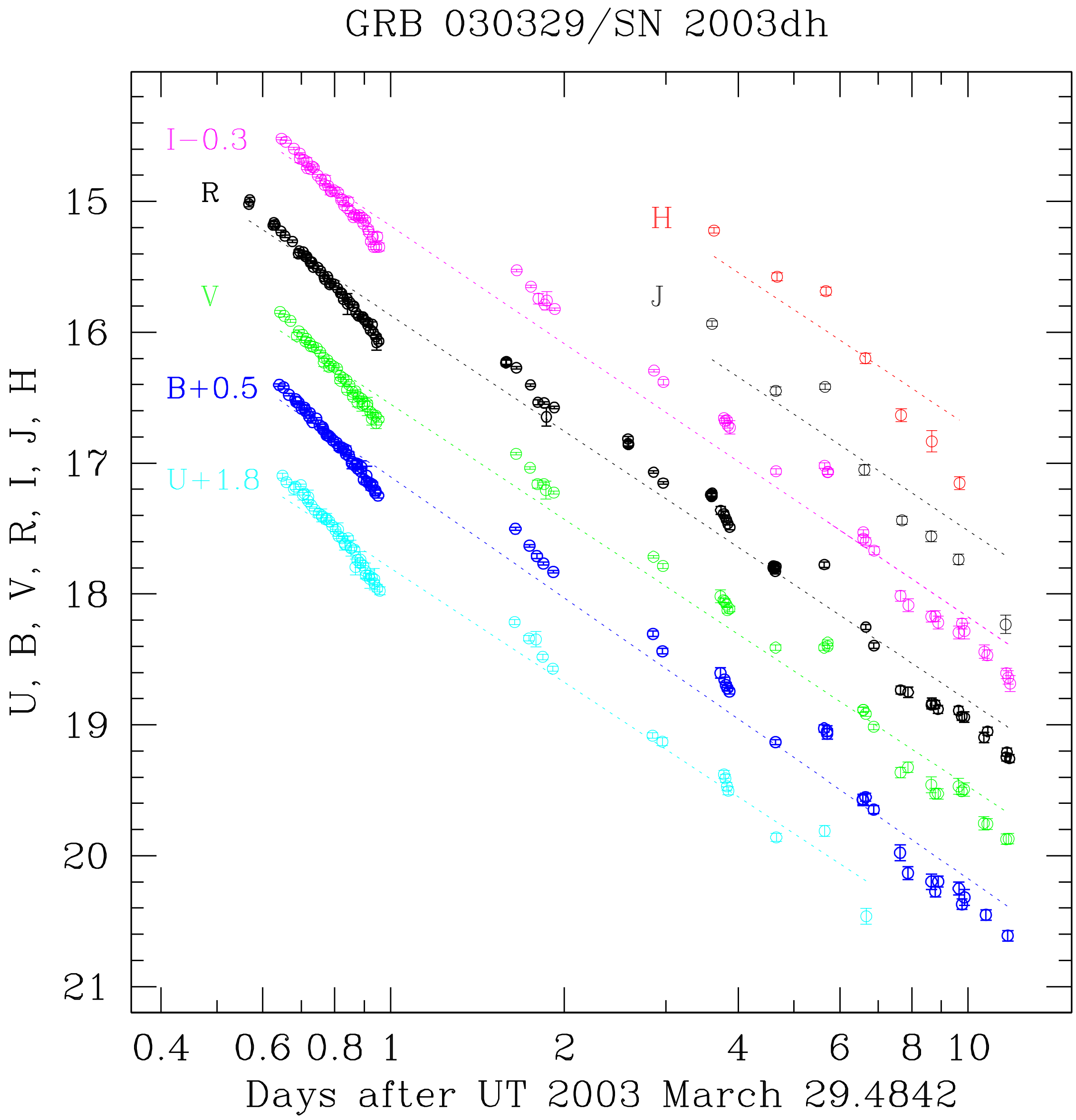

Fig. 1.— Early *UBVRIJH* light curves of GRB 030329/SN 2003dh (based on the data in Table 1). The dotted line for each band is a formal linear fit and is shown only to guide the eye (for J and H, we used the slope of the R-band fit). One clearly sees the bumpy character of the light curve.

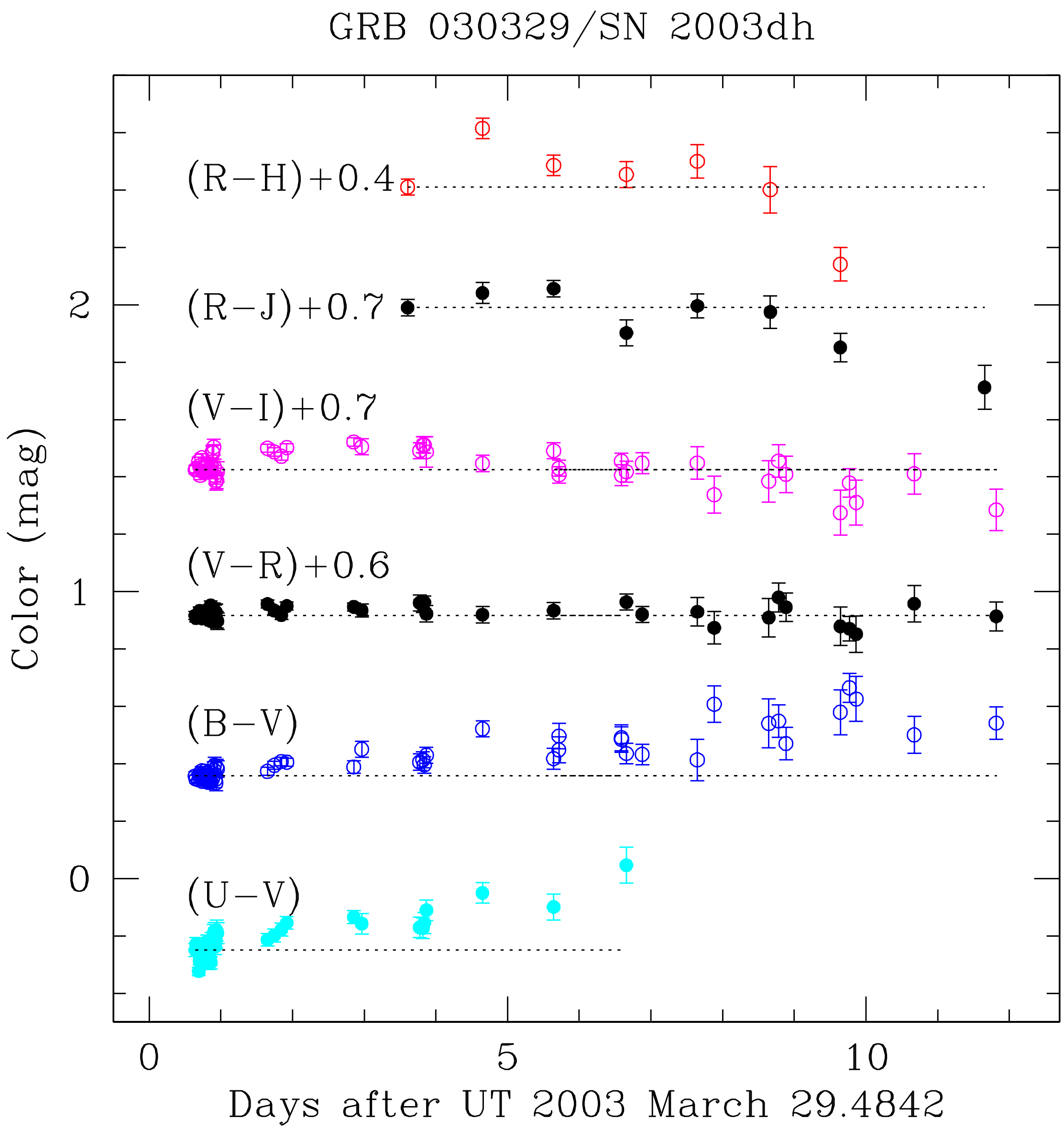

Fig. 2.— Early color evolution of the OT. Fiducial levels (*dotted lines*) represent the value of the first point for each color.

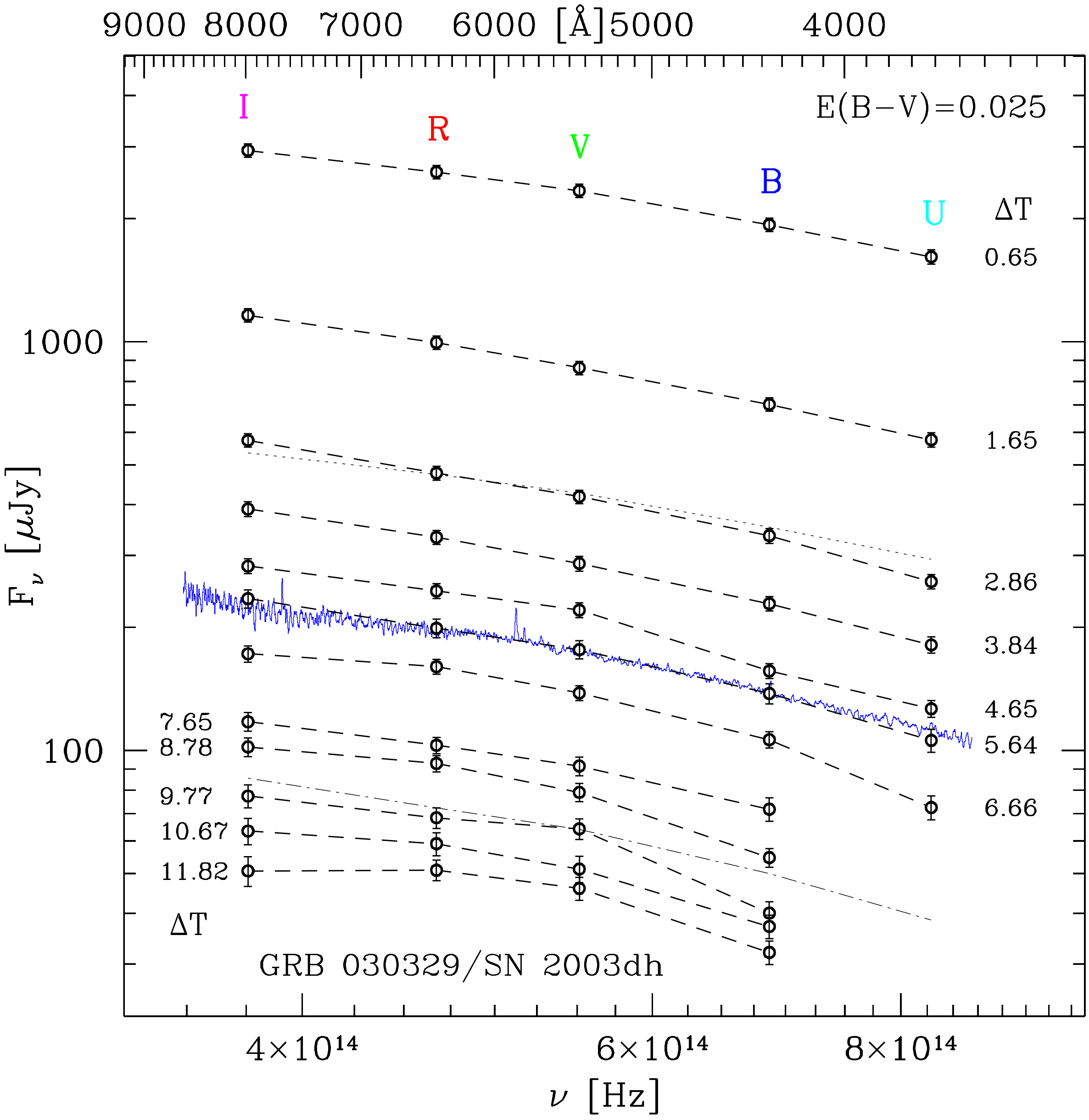

Fig. 3.— Spectral energy distribution (SED) of the optical afterglow of GRB 030329 at various times (indicated on the right side of each SED for nights 1-7 and on the left side for nights 8-12). We superimposed an MMT spectrum obtained nearly simultaneously with our photometry at $\Delta T = 5.64$ days (our fiducial spectrum). The SED from $\Delta T = 0.65$ days is shown (*dotted line*) on top of the SED from $\Delta T = 2.86$ days. The SED from $\Delta T = 5.64$ days is shown (*dash-dotted line*) on top of the SED from $\Delta T = 9.77$ days. For clarity, SEDs from $\Delta T = 5.64, 9.77, 10.67,$ and 11.82 days were multiplied by 0.8.

(where ΔT is the time since the GRB), the red part of the SED (VRI) remains unchanged, while the blue part of the SED (UB) is clearly depressed by about 0.1 mag. On the following epoch, $\Delta T = 5.64$ days, the SED "recovers" and resembles closely the SEDs from nights 3-4. After $\Delta T = 6.66$ days, as discussed below, the supernova component starts to emerge quickly and the colors and SEDs undergo dramatic evolution: while nearly unchanged in $V - R$, the transient becomes more red in $B - V$ and strongly bluer in $R - I$, $R - J$, and $R - H$. Similar color changes at early times (without UJH) were discussed in GCN Circulars by Bersier et al. (2003b) and Henden et al. (2003). This peculiar color change is because the supernova flux peaks around 6000 Å, raising V and R nearly equally while the bands redward and blueward slope up toward the peak.

The "color event" of $\Delta T = 4.65$ days is also present in the near-IR data, as can be seen in Figure 2. To highlight this color change, we show in Figure 4 the evolution of the SED of the optical afterglow of GRB 030329 between $\Delta T = 4.65$ days and $\Delta T = 5.64$ days.

4.2. Early Spectroscopy

The brightness of the OT allowed us to observe the OT each of the 12 nights between March 30 and April 10 UT, mostly with the MMT 6.5-m, but also with the Magellan 6.5-m, Lick Observatory 3-m, LCO du Pont 2.5-m, and FLWO 1.5-m telescopes. This provided a unique opportunity to look for spectroscopic evolution over many nights. The early spectra of the OT of GRB 030329 (top of Figure 5) consist of a power-law continuum typical of GRB afterglows, with narrow emission features identifiable as Hα, [O III] $\lambda\lambda$4959, 5007, Hβ, and [O II] λ3727 at $z = 0.1685$ (Greiner et al. 2003; Caldwell et al. 2003) probably from H II regions in the host galaxy. Assuming a Lambda cosmology with $H_0 = 70$ km s^{-1} Mpc^{-1}, $\Omega_m = 0.3$, and $\Omega_\Lambda = 0.7$, this redshift corresponds to a luminosity distance of 810 Mpc.

Beginning at $\Delta T = 7.67$ days, our spectra deviated from the pure power-law continuum. Broad peaks in flux, characteristic of a supernova, appeared. The broad bumps are seen at approximately 5000 Å and 4200 Å (rest frame). At that time, the spectrum of GRB 030329 looked similar to that of the peculiar Type Ic SN 1998bw a week before maximum light (Patat et al. 2001) superposed on a typical afterglow continuum. Over the next few days the SN features became more prominent as the afterglow faded and the SN brightened toward maximum.

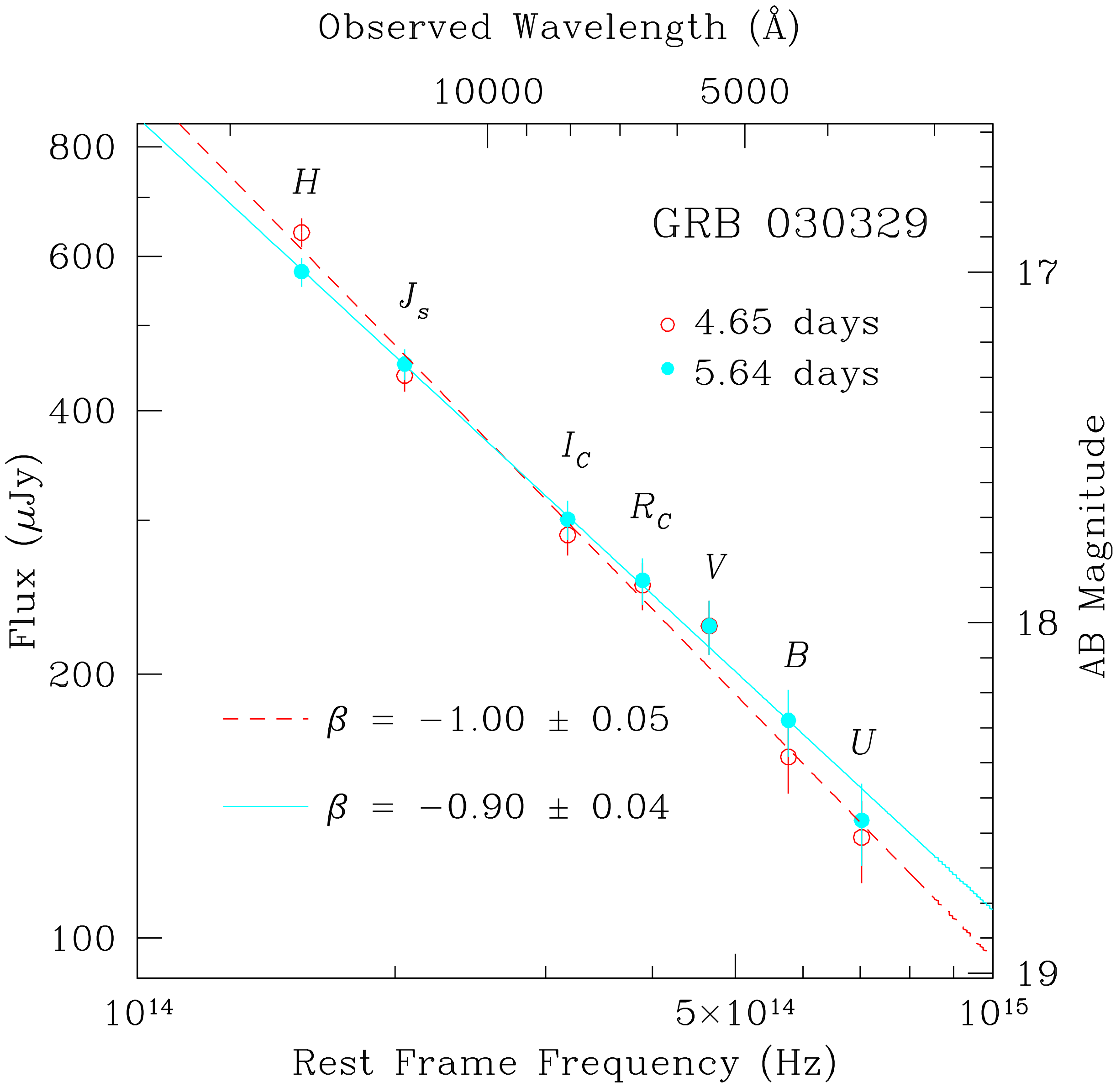

Fig. 4.— Evolution of the SED of the optical afterglow of GRB 030329 between $\Delta T = 4.65$ days (*open circles*) and $\Delta T = 5.64$ days (*filled circles*), the "color event" described in the text.

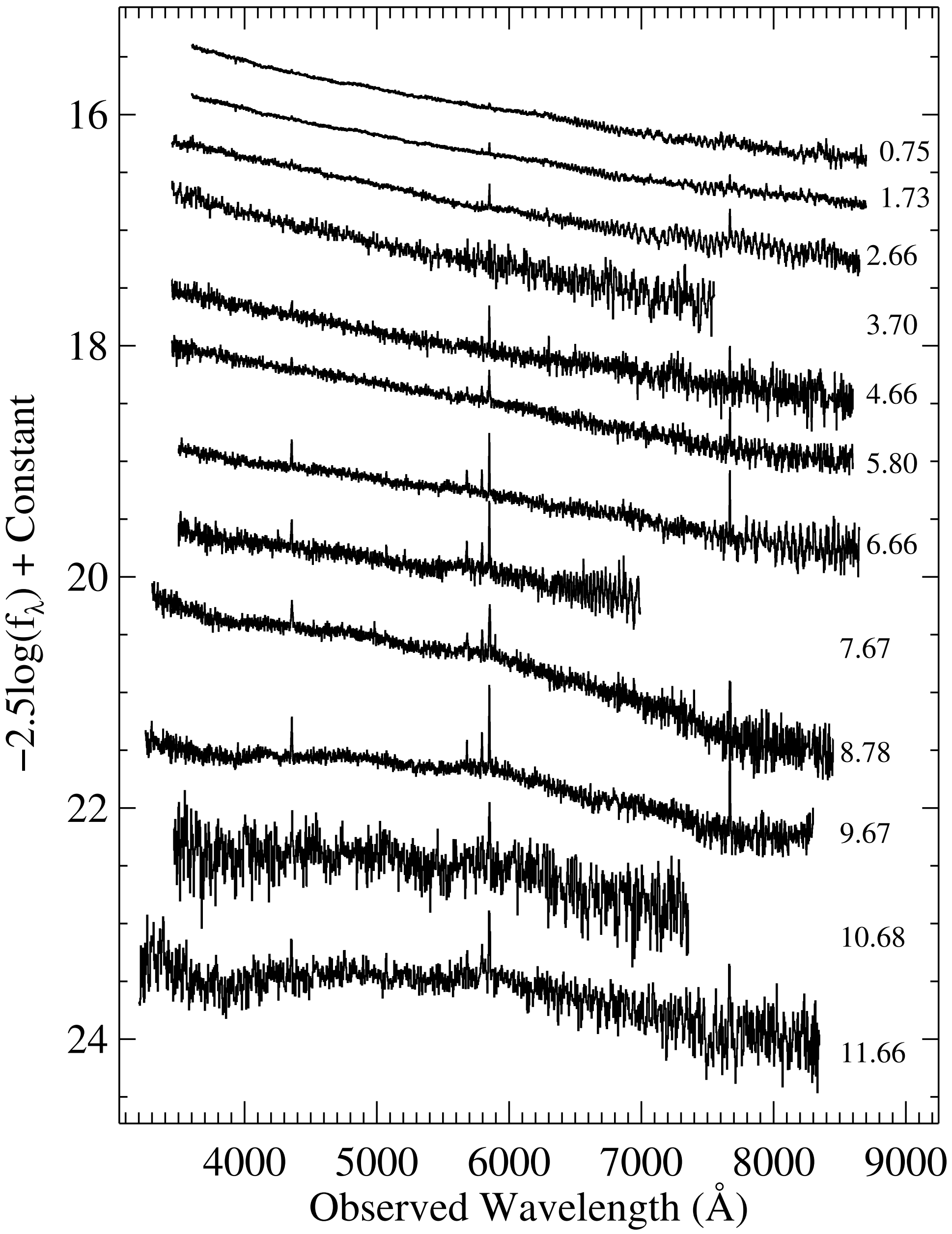

Fig. 5.— Evolution of the GRB 030329/SN 2003dh spectrum, from March 30.23 UT (0.75 days after the burst), to April 10.14 UT (11.66 days after the burst). The early spectra consist of a power-law continuum with narrow emission lines originating from H II regions in the host galaxy at $z = 0.1685$. Spectra taken after $\Delta T = 6.66$ days show the development of broad peaks characteristic of a supernova. In some spectra, regions of bad fringing or low signal-to-noise ratio have been removed for clarity. Spectra from $\Delta T = 3.70, 10.68$, and 11.66 days have been rebinned to improve the signal-to-noise ratio. Note that not all spectra listed in Table 2 are presented in this figure.

5. Later Photometry and Spectroscopy: Days 13-61

5.1. Later Photometry

We continued observing the OT in the R band using mostly the FLWO 1.2-m telescope, and also obtaining some data with the KPNO 4-m and the LCO Swope 1-m telescopes. In the B band, we obtained most of the later data with the KPNO 4-m, and also some data with the du Pont 2.5-m and the FLWO 1.2-m telescopes. The two gaps in the R-band coverage correspond to the Moon being bright or near the position of the OT, and also when the CCD camera was not mounted. The results are shown in Figure 6.

There are several interesting features to be seen in Figure 6. Coinciding with the first detection of the supernova in the spectra, both R and B light curves start to decay more slowly (this can be also seen in Figure 1). In addition, the $(B-R)$ color undergoes a dramatic change at later times, as can be seen in the lower panel of Figure 6. Both of these characteristics result from the supernova component, redder in $(B-R)$ color than the GRB afterglow, strongly contributing to the total light of the OT starting at $\Delta T = 7.67$ days. The strong $(B-R)$ color change indicates that at later times the supernova component dominates the total light, as will be discussed in more detail later in the paper.

Another striking feature is the "Jitter Episode" (Stanek, Latham, & Everett 2003; Stanek et al. 2003c; Ibrahimov et al. 2003) in the late R-band light curve observed between 51.75 and 60.7 days after the burst. The light curve is seen to vary on timescales of ~ 2 days by > 0.3 mag, such as when the OT brightens from $R = 21.70 \pm 0.11$ mag at $\Delta T = 52.71$ days to $R = 21.31 \pm 0.09$ mag at $\Delta T = 54.69$ days, only to fade to $R = 21.61 \pm 0.06$ mag at $\Delta T = 57.72$ days.

We should stress that these data were obtained with exactly the same instrumentation and reduced with the same software and in the same manner as our earlier, much smoother data (see Figure 6). This "Jitter Episode" is unusual when compared to the whole data set and we strongly believe that it is real. We will discuss it in more detail later in the paper.

5.2. Later Spectroscopy

Later spectra obtained on April 24.28, May 2.05, May 4.01, and May 24.38 continue to show the characteristics of a supernova. As the power-law continuum of the GRB afterglow fades, the supernova spectrum rises, becoming the dominant component of the overall spectrum (Figure 7).

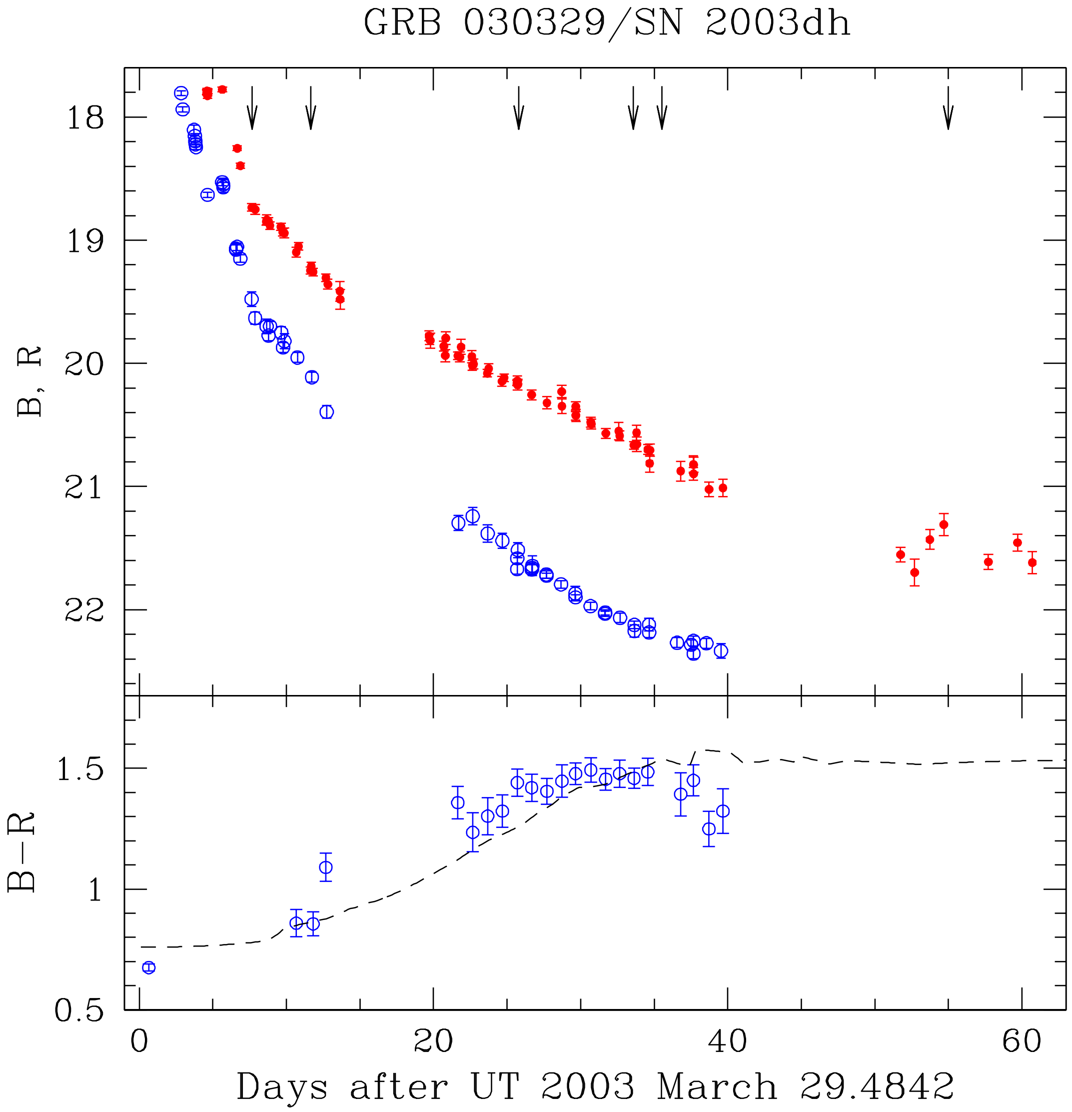

Fig. 6.— Upper panel: B-band (*open circles*) and R-band (*filled circles*) photometry at later times, with the last R-band epoch at $\Delta T = 60.7$ days after the burst. The first two arrows correspond to the first time when the supernova signature could be seen in the spectra and the last spectrum in the continuous series. The remaining arrows correspond to our spectra taken after $\Delta T = 12.0$ days. Lower panel: $B - R$ color evolution in later times. The solid line indicates the color expected for an afterglow with a fixed power-law spectrum plus a supernova like SN 1998bw K-corrected to the redshift of GRB 030329. Contamination from the host galaxy may contribute to the B-band light at late times.

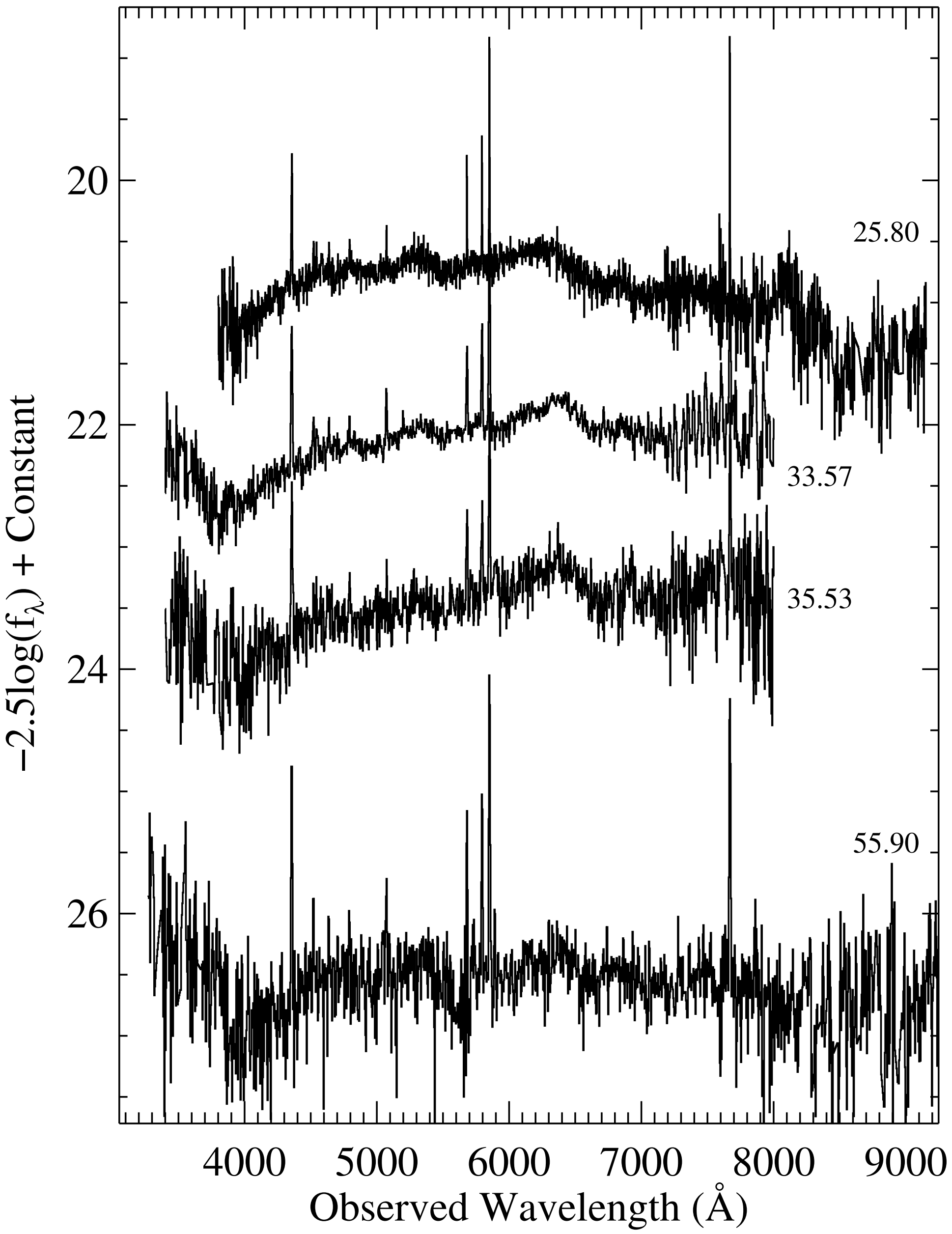

Fig. 7.— Evolution of the GRB 030329/SN 2003dh spectrum, from April 24.28 UT (25.8 days after the burst), to May 24.38 (55.9 days after the burst). The power-law contribution decreases and the spectra become more red as the SN component begins to dominate, although the upturn at blue wavelengths may still be the power law. The broad features of a supernova are readily apparent, and the overall spectrum continues to resemble that of SN 1998bw several days after maximum. The ΔT = 25.8 days spectrum is a combination of the ΔT = 25.71 days MMT spectrum and the ΔT = 25.89 days ESI spectrum. The dip near 5600 Å in the ΔT = 55.90 days spectrum is due to the dichroic used in LRIS, and is not intrinsic to the OT.

6. Analysis

6.1. Properties of the Host

The low redshift of this burst meant that the rest-frame optical spectrum of the host galaxy could be obtained, thus allowing the use of well-tested techniques for measuring the metallicity, reddening, and star-formation rate of the host. The MMT spectra from the nights of 2003 Apr 4, 5, 7, and 8 UT were averaged together and a low-order fit to the continuum was subtracted, since the SN was apparent in the averaged spectrum. At a later date when the optical transient has completely faded, it will be valuable to get a spectrum showing the absorption-line component, but the present spectrum is suitable for studying the emission-line component. *HST* images and spectra (Fruchter et al. 2003) show the host to extend to about $0.5''$, so most of the light of the host galaxy should be contained within the MMT slit used even though the GRB was off center. The Hα flux measured should thus refer to the entire galaxy, at least for those nights where the seeing was good.

Overall, the emission-line spectrum shows strong forbidden oxygen lines and hydrogen Balmer lines, but no detection of the [N II] $\lambda\lambda$6548, 6584 lines, with line ratios indicative of low-metallicity gas photoionized by stars. Table 3 lists the observed ratios, measured using the IRAF "splot" routine. We first estimate the reddening using the Hα/Hβ line-intensity ratio as a measure of the Balmer decrement, assuming Case B recombination (e.g., Osterbrock 1989) and the Whitford extinction law. The redshifted Hα line is affected by telluric absorption, which may have lead to errors in the Hα/Hβ ratio, but the dominant source of error in the line ratios is simply photon counting. The reddening implied by the difference between the observed ratio and the theoretical value is in the range $E(B-V) =$ 0.05 - 0.11 mag. If the Galactic foreground reddening is $E(B-V) = 0.025$ mag (Schlegel et al. 1998), then the reddening intrinsic to the host is in the range 0.03 to 0.09 mag.

To estimate the oxygen abundance in the host, we use the R_{23} method that employs the ratios of [O III]/[O II], [N II]/[O II], and [O II]+[O III]/Hβ (Pagel 1986; Kewley & Dopita 2002). Using a reddening of 0.05 mag to correct the line ratios, and the parameterizations found in Kewley & Dopita, we derive an ionization parameter $q = 2 \times 10^7$ cm s^{-1}, which then leads to an oxygen abundance of log(O/H)+12 = 8.5, or about 0.5 $Z_\odot$. The lack of detectable [N II] is consistent with this moderate metallicity.

The Hα flux was measured from the spectrum of 2003 April 8, and when corrected for reddening, gives an Hα luminosity of $L(\mathrm{H}\alpha) = 6.6 \times 10^{40}$ erg s^{-1}, for a distance of 810 Mpc. This corresponds to a current star formation rate of $7.9 \times 10^{-42}\ L(\mathrm{H}\alpha) = 0.5$ $M_\odot$ yr^{-1} (Kennicutt 1998). This would be a modest star formation rate in a large galaxy, but the host of GRB 030329 is probably a dwarf. Fruchter et al. (2003) estimate the magnitude of the host to be $V = 22.7$, meaning $M_V = -16.9$ mag, which is similar to the luminosity of the SMC. The moderate metallicity we have calculated is in accord with the galaxy luminosity, in this case corresponding well with that of the LMC, which has a metallicity of log(O/H)+12 = 8.4 (Russell & Dopita 1990).

Star formation rates in dwarfs can vary widely. Hunter, Hawley, & Gallagher (1993) report a range of rates from 0.001 to 3 $M_\odot$ yr^{-1}, the latter limit referring to starburst dwarfs such as NGC 1569. The mean value is around 0.03 $M_\odot$ yr^{-1}. A useful comparison of star formation ability in local dwarf galaxies can then be made by calculating the birthrate, the ratio of the current star formation rate to the average past rate. We estimate this quantity simply by normalizing the current rate to the galaxy blue luminosity divided by an age of 12 Gyr, and assuming $M/L = 3$. For the host of GRB 030329, the birthrate is about 5 $M_\odot$ yr^{-1}. That can be compared to the SMC value of 0.3 $M_\odot$ yr^{-1}, and the value of 2 $M_\odot$ yr^{-1} for the starburst galaxy NGC 1569 (derived from data in Hunter et al. 1993 and Kennicutt & Hodge 1986). One is driven to the conclusion that the GRB 030329 host is also a starburst dwarf galaxy.

The more massive hosts of other GRBs also show large star formation rates, particularly when measured via radio or sub-mm techniques. Berger et al. (2003) calculate rates of 100-500 $M_\odot$ yr^{-1} in bolometrically luminous hosts ($L > 10^{12}$ $L_\odot$). However, the rates derived from an optical emission line ([O II] λ3727) for other GRB hosts are much lower, $1 - 10$ $M_\odot$ yr^{-1} (Djorgovski et al. 2001). The discrepancy in rates is not yet understood, particularly since the extinction measured in the optical for the Djorgovski hosts is low, as we have found here. Sub-mm observations of the host of GRB 030329 would be interesting in this regard.

6.2. Extinction Toward the GRB in the Host

We used our $UBVR_CI_CJ_sH$ photometry from $\Delta T = 5.64$ days after the burst to investigate whether there is any evidence for extinction in the host galaxy along the line of sight to GRB 030329/SN 2003dh. The optical and infrared magnitudes were converted to flux densities based on the AB corrections given in Fukugita et al. (1995) and Mégessier (1995). Each data point was corrected for a small Galactic reddening of $E(B - V) = 0.025 \pm 0.020$ mag (Schlegel et al. 1998). No corrections were applied for any reddening that may be present in the host galaxy or in intergalactic space between us and the host.

The spectral energy distribution was fit by $f_\nu(\nu) \propto \nu^\beta \times 10^{-0.4A(\nu)}$, where $f_\nu(\nu)$ is the flux density at frequency ν, β is the intrinsic spectral index, and $A(\nu)$ is the extragalactic extinction along the line of sight to the burst. The dependence of $A(\nu)$ on ν has been parameterized in terms of the rest-frame A_B following the three extinction laws given by Pei (1992) for the Milky Way (MW), the Large Magellanic Cloud (LMC), and the Small Magellanic Cloud (SMC). The fit provides β and A_B simultaneously for each of the assumed extinction laws. The unextinguished case ($A_B = 0$) was also considered.

The best fit is for an SMC extinction law with $A_B = 0.16 \pm 0.30$ mag of extinction in the host and an intrinsic spectral slope of $\beta = -0.80 \pm 0.20$ (χ^2/DOF $= 0.267$). All three extinction laws of Pei (1992) give fits that are statistically similar(χ^2/DOF $= 0.267$–0.282) and consistent with $A_B = 0.16$ mag and $\beta = -0.80$. Therefore we are unable to constrain the form of the extinction law in the host. This slope is also consistent with the no extinction case ($A_B = 0$ with χ^2/DOF $= 0.273$). Therefore, we conclude that there is no strong evidence for extragalactic dust along the line of sight between us and GRB 030329. Figure 8 shows the SED at 5.64 days along with fits for an SMC extinction law and no extinction. To test for dust along the line of sight between us and the host we repeated our fits allowing the redshift of the dust to be a free parameter. The best fit was for $z = 0.00 \pm 0.09$ with $A_B = 0.17 \pm 0.31$ mag and $\beta = -0.81 \pm 0.18$ (χ^2/DOF $= 0.352$).

The most likely distribution for the dust is an SMC extinction law with $A_B = 0.16 \pm 0.30$ mag in the host galaxy, which corresponds to $A_V = 0.12 \pm 0.22$ mag and $E_{B-V} = 0.04 \pm 0.08$ mag in the rest frame of the host. Note that this is consistent with the reddening derived from line ratios in the previous section.

6.3. Evidence for a Cooling Break

Price et al. (2003) find that the slope of the optical decay increases from $\alpha = -0.87 \pm 0.03$ to $\alpha = 1.97 \pm 0.12$ approximately 0.5 days after the burst. If their interpretation of this as evidence for a jet break is correct, then the expected electron index is $p \approx 2$ since $\alpha = p$ after the jet break has occurred. Tiengo et al. (2003) report that *Rossi-XTE* X-ray observations yield an X-ray spectrum with a slope of $\beta_X = -1.17^{-0.04}_{-0.03}$ and an X-ray flux decay of $\alpha_X = -0.9 \pm 0.3$ at 0.25 days after the burst. Using the relationships of Sari et al. (1999) and Chevalier & Li (1999) we can rule out the case where the cooling frequency, ν_c, is above the X-ray band since the observed α_X and β_X predict different values for the electron index, p. Therefore, the cooling break must be between the lower edge of the *Rossi-XTE* X-ray band (0.2 keV) and the R band at this time. The optical and X-ray decay indices and the X-ray spectral index at 0.25 days are consistent with $p = 2.2 \pm 0.1$, which is consistent with the observed decay index after the jet break.

The spectral index computed in Section 4.1 for 0.65 days after the burst predicts $p = 1.4$

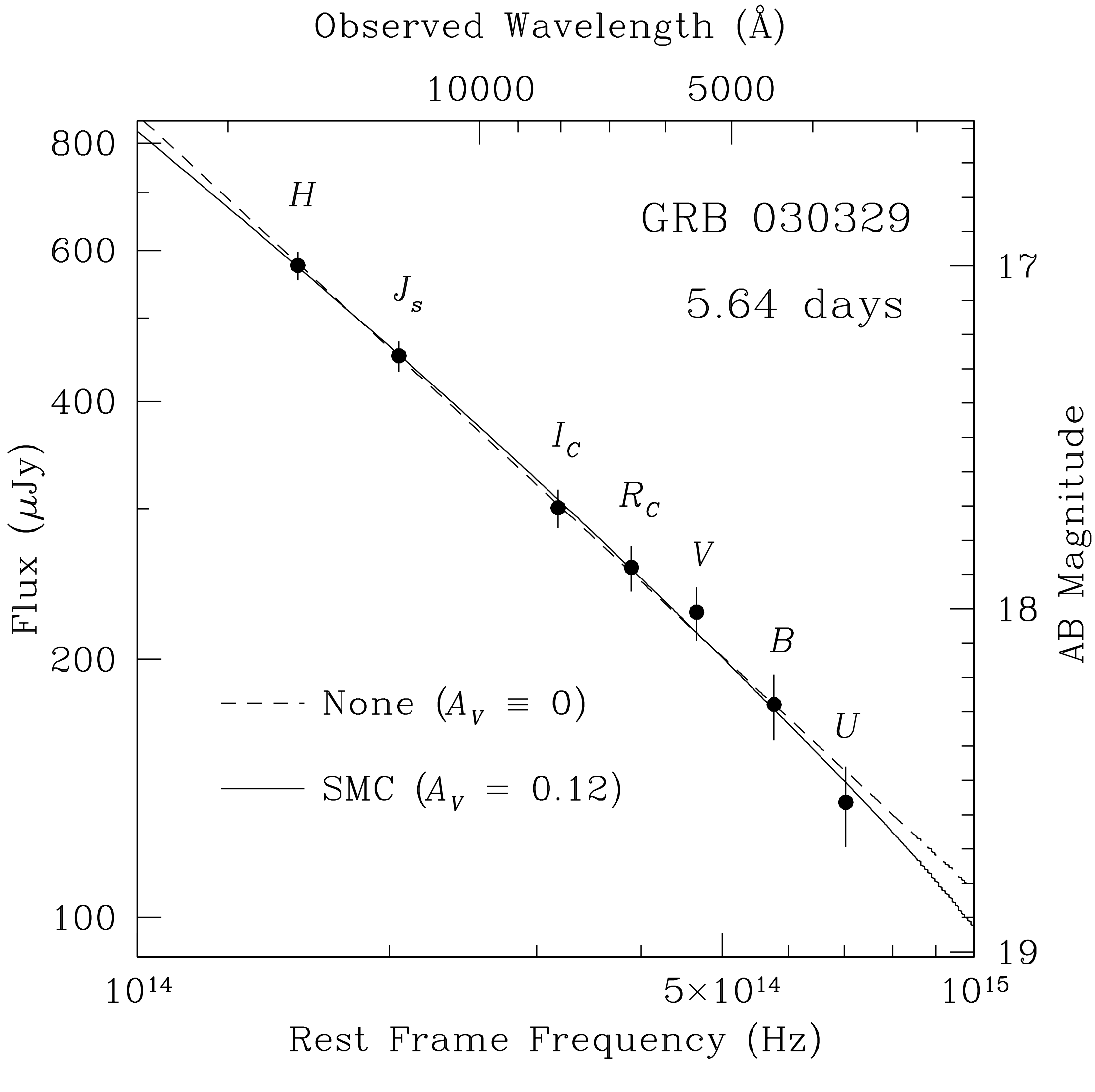

Fig. 8.— Spectral energy distribution of the optical afterglow of GRB 030329/SN 2003dh at $\Delta T = 5.64$ days after the burst. The filled circles represent observed photometry corrected for extinction in the Milky Way and shifted to the rest frame of the host galaxy. The lines represent the best-fitting spectral energy distribution, assuming an SMC extinction law (*solid line*) or no extinction (*dashed line*). If we assume that the unextinguished spectrum follows $f_\nu(\nu) \propto \nu^\beta$ then the best fit has $\beta_0 = -0.80 \pm 0.20$ and $A_B = 0.16 \pm 0.30$ mag.

if the cooling break frequency is below the optical and $p = 2.4$ if it is above the optical. Values for the electron index of less than two represent infinite energy in the electrons. This strongly suggests that $\nu_c > \nu_R$ at this time. However, at $1.65 \leq \Delta T \leq 5.64$ days the optical spectral slopes (see Section 4.1) are consistent with $\nu_c < \nu_R$ and $p \approx 2$. The case where $\nu_c > \nu_R$ at these times implies $p \approx 3$, which is inconsistent with the value of the electron index that was derived for $\Delta T = 0.25$ days. Tiengo et al. (2003) used *XMM-Newton* X-ray observations to find $\beta_X = -0.92^{+0.26}_{-0.15}$ at 37 days and $\beta = -1.1^{+0.4}_{-0.2}$ at 61 days. Both of these are consistent with $p \approx 2$ and $\nu_c < \nu_R$. Therefore we believe that the cooling break passed through the optical, moving toward radio frequencies, between 0.65 and 1.65 days after the burst. A cooling frequency that decreases with time is the hallmark of a homogeneous interstellar medium. However, there may be local inhomogeneities on scales that are small compared to the size of the fireball.

At X-ray frequencies interstellar absorption does not significantly affect the slope of the spectrum, so the observed slope is a good approximation of the actual slope. Combining all of the β_X values from Tiengo et al. (2003) yields $p = 2.2 \pm 0.1$. This predicts that the optical spectrum has $\beta = -1.10 \pm 0.05$ at $\Delta T = 5.64$ days, which is close to the observed spectrum. This agreement strengthens our conclusion in Section 6.2 that there is no strong evidence for dust in the host galaxy along the line of sight to the burst.

6.4. Separating the GRB from the Supernova

To explore the nature of the supernova underlying the OT, we modeled the spectrum as the sum of a power-law continuum and a peculiar Type Ic SN. Specifically, we chose for comparison SN 1998bw (Patat et al. 2001), SN 1997ef (Iwamoto et al. 2000), and SN 2002ap (using our own as yet unpublished spectra, but see, e.g., Kinugasa et al. 2002; Foley et al. 2003). We had 62 spectra of these three SNe, spanning the epochs of seven days before maximum to several weeks past. For the power-law continuum, we chose to use one of our early spectra to represent the afterglow of the GRB. The spectrum at time $\Delta T = 5.80$ days was of high signal-to-noise ratio (S/N), and suffers from little fringing at the red end. Therefore, we smoothed this spectrum to provide the fiducial power-law continuum of the OT for our model. Other choices for the continuum did not affect our results significantly.

To find the best match with a supernova spectrum, we compared each spectrum of the afterglow with the sum of the fiducial continuum and a spectrum of one of the SNe in the sample, both scaled in flux to match the OT spectra. We performed a least-squares fit, allowing the fraction of continuum and SN to vary, finding the best combination of continuum and SN for each of the SN spectra. The minimum least-squares deviation within this set was then taken as the best SN match for that epoch of OT observation. The results of the fits for the spectra we modeled are listed in Table 4. Figure 9 shows the relative contribution to the OT spectrum by the underlying SN in the B and R bands as a function of ΔT.

Within the uncertainties of our fit, the SN fraction is consistent with zero for the first few days after the GRB. At $\Delta T = 7.67$ days, the SN begins to appear in the spectrum, without strong evidence for a supernova component before this. Hjorth et al. (2003) report evidence for the SN spectrum in their April 3 UT data ($\Delta T \approx 4$ days), but we do not see any sign of a SN component at this time. There is a color change near $\Delta T \approx 5$ days as noted above (see also Figure 3), but we attribute it to the afterglow. Our decomposition of the photometry into SN and afterglow components (see below) indicates that, at most, the SN would have contributed only a few percent of the total light at this point, making it difficult to identify indisputable features.

Note that when the fit indicates the presence of a supernova, the best match is almost always SN 1998bw. The only exceptions to this are from nights when the spectrum of the OT are extremely noisy, implying that less weight should be given to those results. The least-squares deviation for the spectra that do not match SN 1998bw is also much larger (see Table 4).

Our best spectrum (i.e., with the highest S/N) from this time when the SN features begin to appear is at $\Delta T = 9.67$ days. In Figure 10, our best fit of 74% continuum and 26% SN 1998bw (at day -6 relative to SN B-band maximum) is plotted over the observed spectrum from this epoch. The next-best fit is SN 1998bw at day -7. Using a different early epoch to define the reference continuum does not alter these results significantly. It causes slight changes in the relative percentages, but the same SN spectrum still produces the best fit, albeit with a larger least-squares deviation.

The SN fraction contributing to the total spectrum increases steadily with time. By $\Delta T = 25.8$ days, the SN fraction is $\sim 61\%$, with the best-fit SN being SN 1998bw at day $+6$ (Figure 11). The SN percentage at $\Delta T = 33.6$ days is still about 63%, but the best match is now SN 1998bw at day $+13$ (Figure 12). The rest-frame time difference between $\Delta T = 9.67$ days and $\Delta T = 25.8$ days is 13.8 days ($z = 0.1685$). For the best-fit SN spectra from those epochs, SN 1998bw at day -6 and SN 1998bw at day $+6$ respectively, the time difference is 12 days. The rest-frame time difference between $\Delta T = 25.8$ days and $\Delta T = 33.6$ days is 6.7 days, with a time difference between the best-fit spectra for those epochs of 7 days. The spectral evolution determined from these fits indicates that SN 2003dh follows SN 1998bw closely, and it is not as similar to SN 1997ef or SN 2002ap. The analysis by Kawabata et al. (2003) of their May 10 spectrum gives a phase for the spectrum of SN 2003dh that is consistent with our dates, although they do consider SN 1997ef as a viable alternative to

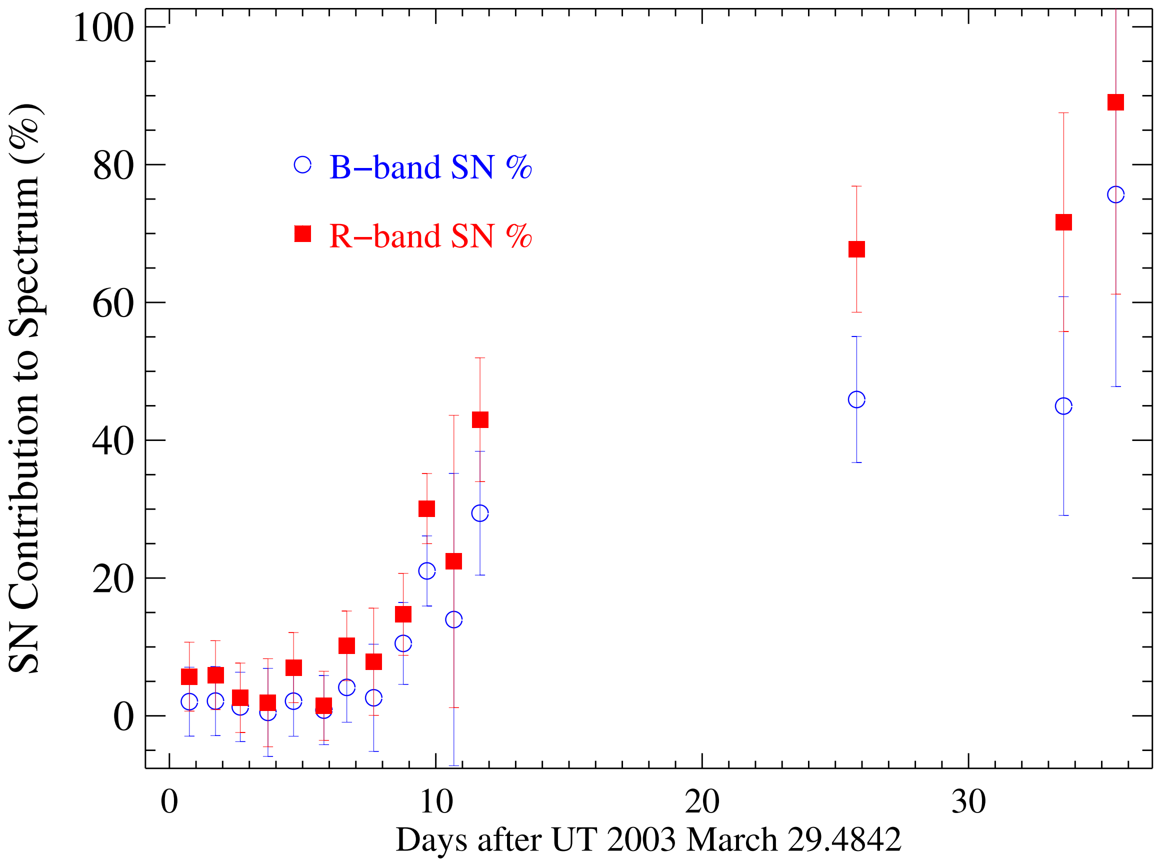

Fig. 9.— Relative contribution of a supernova spectrum to the GRB 030329/SN 2003dh afterglow as a function of time in the B (*open circles*) and R (*filled squares*) bands. Using the technique described in the text, we derive a best fit to the afterglow spectrum at each epoch with the fiducial power-law continuum and the closest match from our set of peculiar SNe Ic. We then synthesize the relative B-band and R-band contributions. There is some scatter for the early epochs due to noise in the spectra, but a clear deviation is evident starting at $\Delta T = 7.67$ days, with a subsequent rapid increase in the fraction of the overall spectrum contributed by the SN. Errors are estimated from the scatter when the SN component is close to zero ($\Delta T < 6$ days) and from the scale of the error in the least-squares minimization.

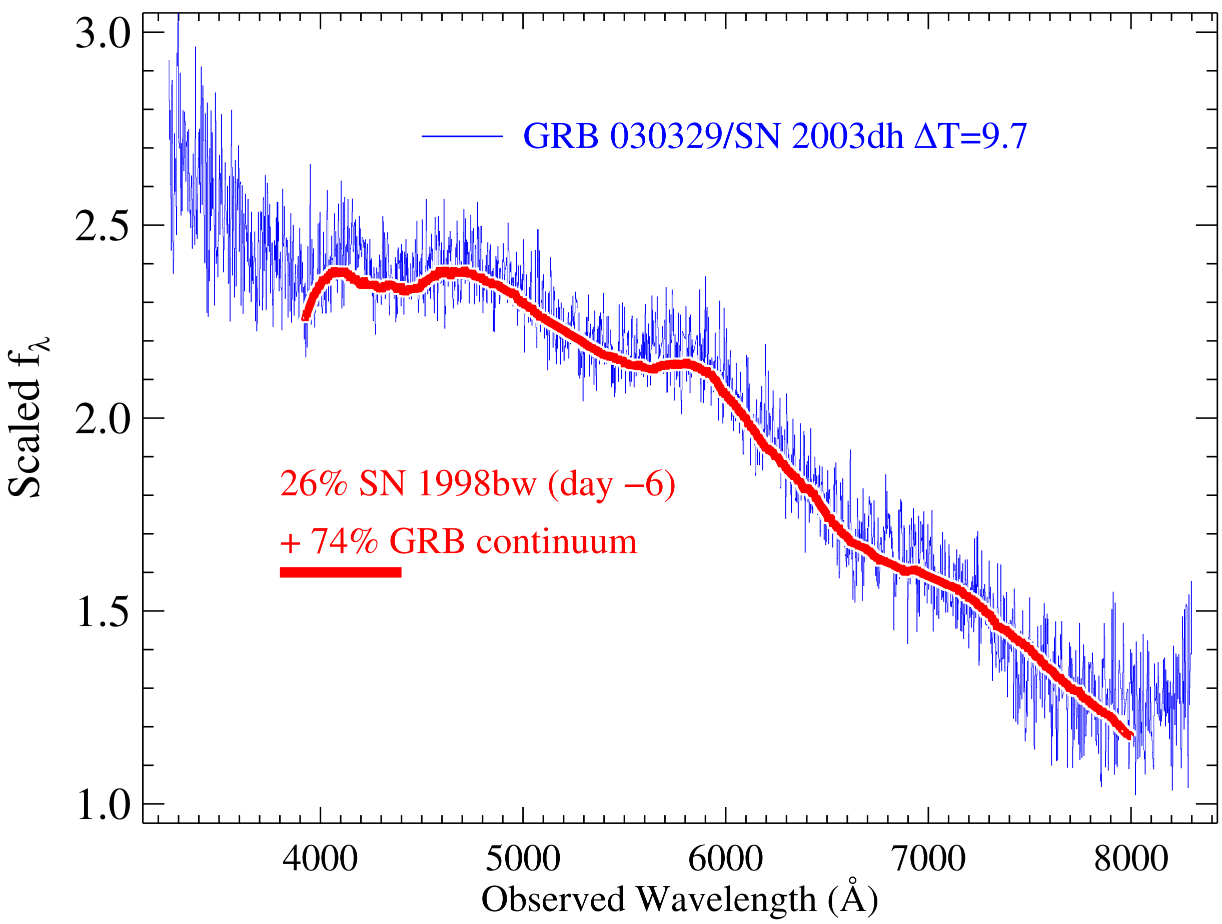

Fig. 10.— Observed spectrum (*thin line*) of the GRB 030329/SN 2003dh afterglow at $\Delta T =$ 9.67 days. The model spectrum (*thick line*) consists of 74% continuum and 26% SN 1998bw from 6 days before maximum. No other peculiar SN Ic spectrum provided as good a fit.

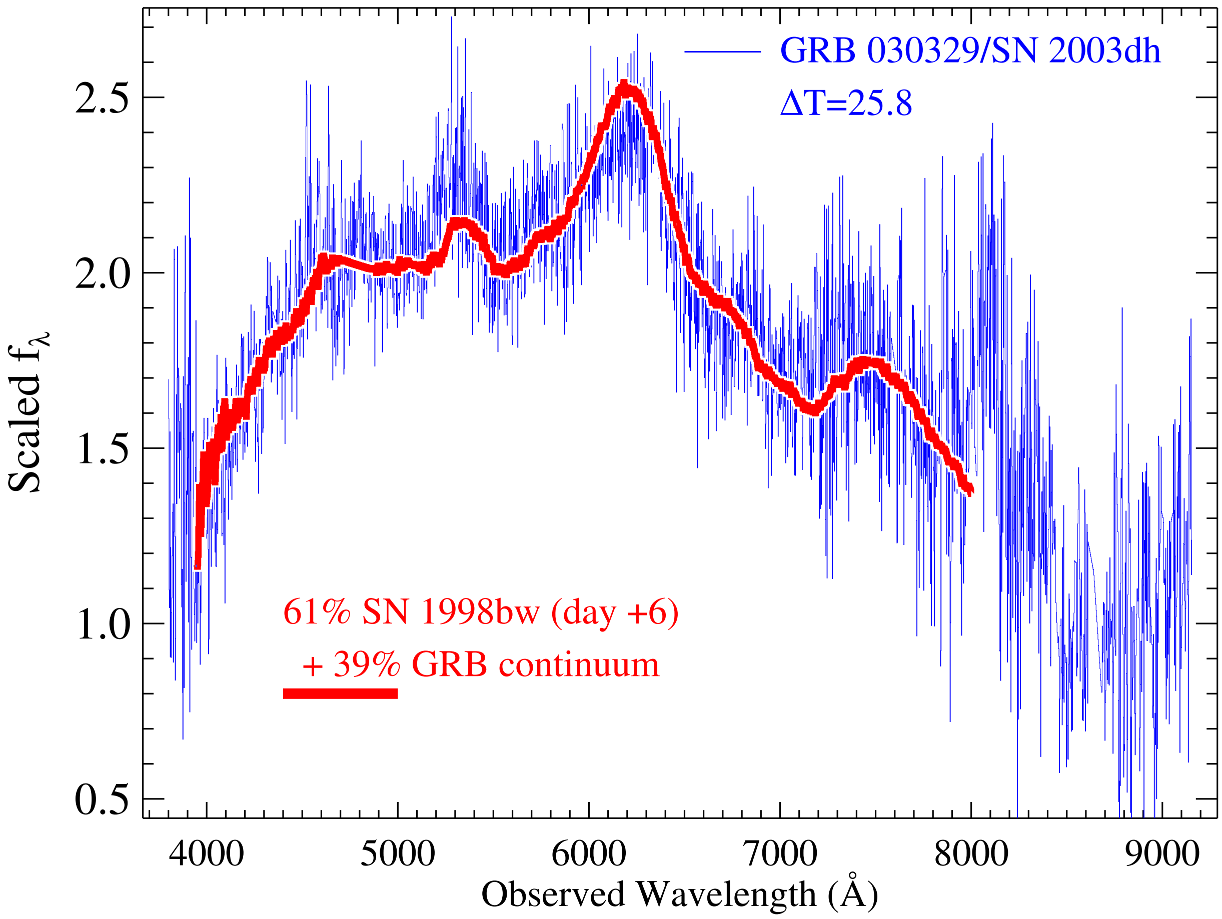

Fig. 11.— Observed spectrum (*thin line*) of the GRB 030329/SN 2003dh afterglow at $\Delta T =$ 25.8 days. The model spectrum (*thick line*) consists of 39% continuum and 61% SN 1998bw from 6 days after maximum.

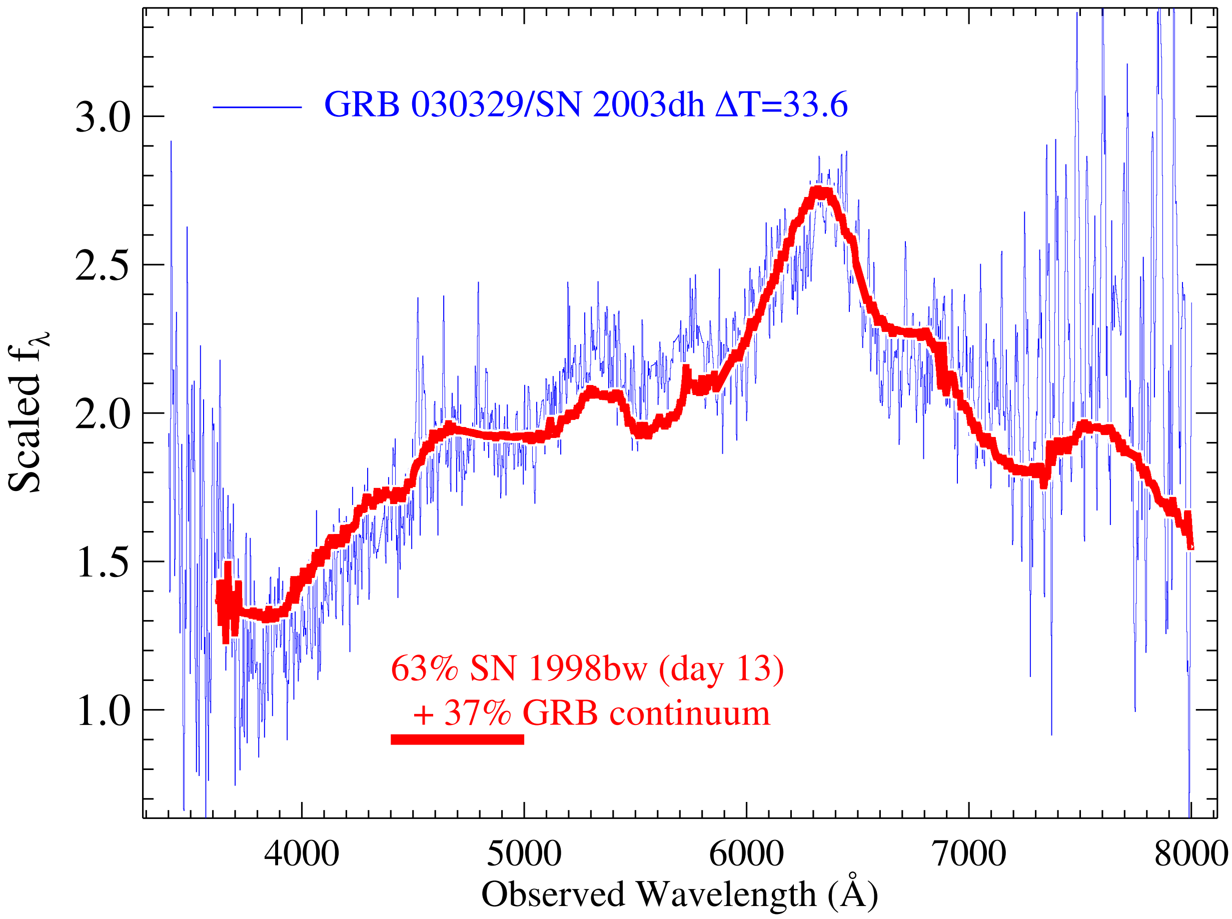

Fig. 12.— Observed spectrum (*thin line*) of the GRB 030329/SN 2003dh afterglow at $\Delta T =$ 33.6 days. The model spectrum (*thick line*) consists of 37% continuum and 63% SN 1998bw from 13 days after maximum.

SN 1998bw as a match for the SN component in the afterglow.

Once the spectrum of the SN has been separated from the power-law continuum of the afterglow, one can consider the nature of SN 2003dh itself. The spectrum does not show any sign of broad hydrogen lines, eliminating the Type II classification, nor is there the deep Si II $\lambda6355$ (usually blueshifted to $\sim$6150 Å) feature that is the hallmark of Type Ia SNe. The optical helium line absorptions that indicate SNe of Type Ib are not apparent either. This leads to a classification of SN 2003dh as a Type Ic (see Filippenko 1997 for a review of supernova classification). Given the striking correspondence with the Type Ic SN 1998bw shown above, this is a natural classification for SN 2003dh.

The spectra of SN 1998bw (and other highly energetic SNe) are not simple to interpret. The high expansion velocities result in many overlapping lines so that identification of specific line features is problematic for the early phases of spectral evolution (see, e.g., Iwamoto et al. 1998; Stathakis et al. 2000; Nakamura et al. 2001; Patat et al. 2001). This includes spectra up to two weeks after maximum, approximately the same epochs covered by our spectra of SN 2003dh. In fact, as Iwamoto et al. (1998) showed, the spectra at these phases do not show line features. The peaks in the spectra are due to gaps in opacity, not individual spectral lines. Detailed modeling of the spectra can reveal some aspects of the composition of the ejecta (e.g., Nakamura et al. 2001). Such a model is beyond the scope of this paper, but the spectra discussed herein and the spectrum of Kawabata et al. (2003) are being analyzed for a future paper (Mazzali et al., in preparation).

If the $\Delta T = 9.67$ days spectrum for the afterglow does match SN 1998bw at day -6, then limits can be placed on the timing of the supernova explosion relative to the GRB. The rest-frame time for $\Delta T = 9.67$ days is 8.2 days, implying that the time of the GRB would correspond to $\sim$14 days before maximum for the SN. The rise times of SNe Ic are not well determined, especially for the small subset of peculiar ones. Stritzinger et al. (2002) found the rise time of the Type Ib/c SN 1999ex was $\sim$18 days (in the B band), while Richmond et al. (1996) reported a rise time of $\sim$12 days (in the V band) for the Type Ic SN 1994I. A rise time of $\sim$14 days for SN 2003dh is certainly a reasonable number. It also makes it extremely unlikely that the SN exploded significantly earlier or later than the time of the GRB, most likely within $\pm$2 days of the GRB itself.

The totality of data contained in this paper allows us to attempt to decompose the light curve of the OT into the supernova and the afterglow (power-law) component. From the spectral decomposition procedure described above, we have the fraction of light in the BR-bands for both components at various times, assuming that the spectrum of the afterglow did not evolve since $\Delta T = 5.64$ days. As we find that the spectral evolution is remarkably close to that of SN 1998bw, we model the R-band supernova component with the V-band light curve of SN 1998bw (Galama et al. 1998a, b) stretched by $(1+z) = 1.1685$ and shifted in magnitude to obtain a good fit. The afterglow component is fit by using the early points starting at $\Delta T = 5.64$ days with late points obtained via the spectral decomposition. This can be done in both in the B and in the R-band and leads to consistent results, indicating that our assumption of the afterglow not evolving in color at later times is indeed valid.

The result of the decomposition of the OT R-band light curve into the supernova and the power-law continuum is shown in Figure 13. The overall fit is remarkably good, given the assumptions (such as using the stretched V-band light curve of SN 1998bw as a proxy for the SN 2003dh R-band light curve). No time offset between the supernova and the GRB was applied, and given how good the fit is, we decided not to explore time offset as an additional parameter. Introducing such an additional parameter would most likely result in a somewhat better fit (indeed, we find that to be the case for $\delta t \approx -2$ days), but this could easily be an artifact with no physical significance, purely due to small differences between SN 1998bw and SN 2003dh. At this point the assumption that the GRB and the SN happened at the same time seems most natural.

6.5. The "Jitter Episode"

We also want to discuss briefly the "Jitter Episode" mentioned earlier (Figure 6). Variations of $> 30\%$ on timescales of ~ 2 days more than 50 days after the burst (> 40 days in the rest frame) are unlikely to be in the supernova component, as such variations have never been observed in any other supernova. It is much more likely that the afterglow of the GRB has exhibited another episode of re-brightening, possibly due to interaction with SN1987A-like rings ejected long ago from the progenitor. Alternatively, the early afterglow had a complicated light curve, possibly due to refreshed shocks (Granot, Nakar, & Piran 2003), and this late "Jitter Episode" could be somehow related to that earlier behavior. An extrapolation of the afterglow light implies that it was more than a magnitude fainter than the supernova two months after the burst so that the afterglow must have varied by nearly a factor of two in brightness. A full investigation of that phenomenon is outside the scope of the current paper, but we should note that its presence complicates the search in the late light curve for the radioactive decay component of the supernova, which could end up being masked by the afterglow component. We continue observing this fascinating event and will report future results in a paper by Bersier et al. (in preparation).

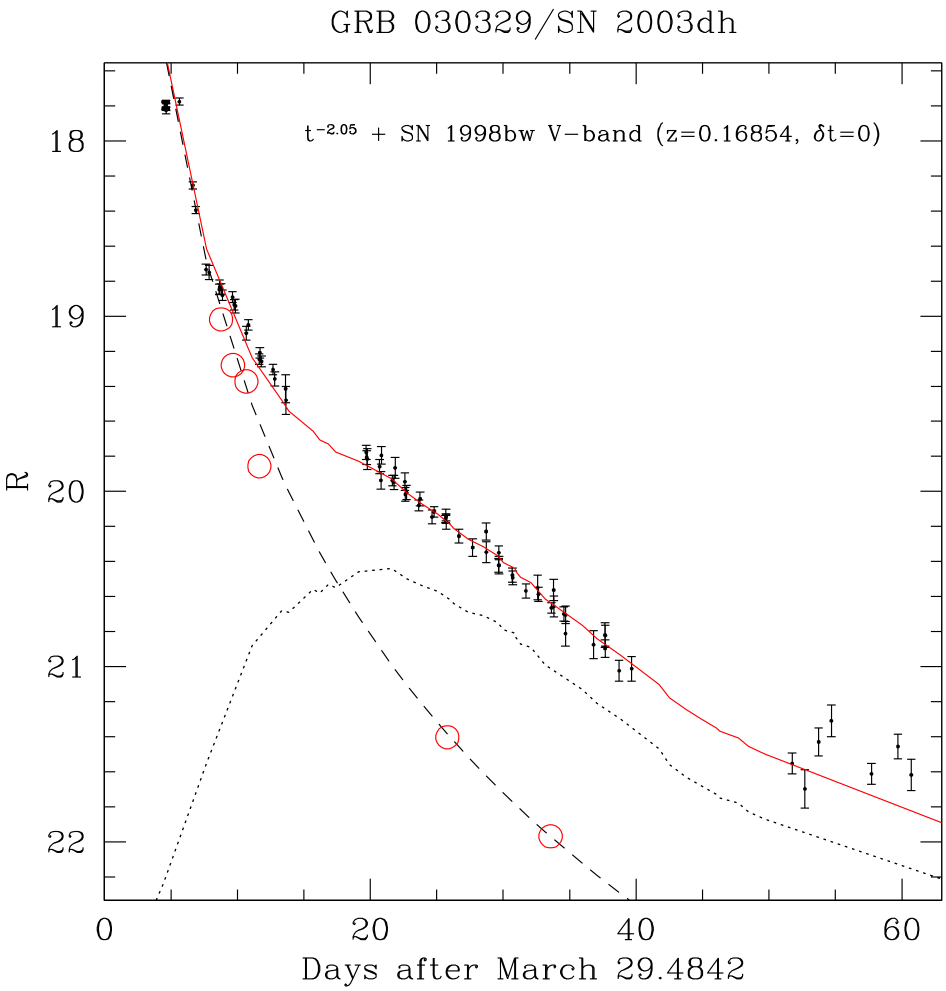

Fig. 13.— Decomposition of the OT R-band light curve into the supernova (*dotted line*) and the power-law continuum (*dashed line*). As the light curve model for the supernova, we took the V-band light curve of SN 1998bw (Galama et al. 1998a, b) stretched by $(1+z) = 1.1685$ and shifted in magnitude. The resulting supernova light curve peaks at an apparent magnitude of $m_R = 20.4$. No offset in time has been applied between the GRB and the supernova. To constrain the continuum, information from the spectral decomposition was used (*big open circles*). See Section 6.4 for discussion.

7. Summary

We have presented optical and infrared photometry and optical spectroscopy of GRB 030329/SN 2003dh covering the first two months of its evolution. The early photometry shows a fairly complicated light curve that cannot be simply fit in the manner of typical optical afterglows. Color changes are apparent in the early stages of the afterglow, even before the supernova component begins to make a contribution. These color changes have been seen in other afterglows (Matheson et al. 2003c; Bersier et al. 2003a), but the physical mechanism that produces them is still a mystery.

At late times, the photometry becomes dominated by the SN component, following the light curve of SN 1998bw fairly well. The colors change distinctly when the SN emerges, although from the light curves alone, there is no clear bump from the SN as has been seen in higher-redshift bursts. There is the "Jitter Episode" near the two-month mark, indicating that the afterglow may still contribute significantly to the observed brightness even at this late date.

The evidence from photometry alone would not be a completely convincing case for the presence of a supernova. The spectra, especially the day-by-day coverage for the first twelve days of the burst, show the transition from the power-law continuum of the afterglow to the broad features characteristic of a supernova. By subtracting off the continuum, the SN becomes directly apparent, and the correspondence with SN 1998bw at virtually all of the epochs for which we have spectroscopy is striking. Taking into account the cosmological time dilation, the development of SN 2003dh follows that of SN 1998bw almost exactly. Using the spectroscopic decomposition of our data, we can separate the light curve into afterglow and SN components, again showing that SN 2003dh follows SN 1998bw. The decomposition suggests that the supernova explosion occurred close to the time of the gamma-ray burst.

The spectroscopy of the optical afterglow of GRB 030329, as first shown by Stanek et al. (2003a), provided direct evidence that at least some of the long-burst GRBs are related to core-collapse SNe. We have shown with a larger set of data that the SN component is similar to SN 1998bw, an unusual Type Ic SN. It is not clear yet whether all long-burst GRBs arise from SNe. Catching another GRB at a redshift this low is unlikely, but large telescopes may be able to discern SNe in some of the relatively nearby bursts. With this one example, though, we now have solid evidence that some GRBs and SNe have the same progenitors.

We would like to thank the staffs of the MMT, FLWO, Las Campanas, Lick, Keck, and Kitt Peak National Observatories. We are grateful to J. McAfee and A. Milone for helping with the MMT spectra. We thank the *HETE2* team, Scott Barthelmy, and the GRB Coordinates Network (GCN) for the quick turnaround in providing precise GRB positions to the astronomical community. We also thank all the observers who provided their data and analysis through the GCN. KPNO, a part of the National Optical Astronomy Observatory, is operated by the Association of Universities for Research in Astronomy, Inc. (AURA), under a cooperative agreement with the National Science Foundation. PMG and STH acknowledge the support of NASA/LTSA grant NAG5-9364. DJE was supported by NSF grant AST-0098577 and by an Alfred P. Sloan Research Fellowship. DM, LI and JM are supported by FONDAP Center for Astrophysics 15010003. JK was supported by KBN grant 5P03D004.21. JCL acknowledges financial support from NSF grant AST-9900789. PM was supported by a Carnegie Starr Fellowship. EWO was partially supported by NSF grant AST 0098518. BP is supported by NASA grant NAG5-9274. RAW and RAJ are supported by NASA Grant NAG5-12460. DCL acknowledges financial support provided by NASA through grant GO-9155 from the Space Telescope Science Institute, which is operated by the Association of Universities for Research in Astronomy, Inc., under NASA contract NAS 5-26555. The work of AVF's group at the University of California, Berkeley, is supported by NSF grant AST-0307894, as well as by the Sylvia and Jim Katzman Foundation. KAIT was made possible by generous donations from Sun Microsystems, Inc., the Hewlett-Packard Company, AutoScope Corporation, Lick Observatory, the NSF, the University of California, and the Katzman Foundation.

REFERENCES

Alard, C. 2000, A&AS, 144, 363

Alard, C., & Lupton, R. 1998, ApJ, 503, 325

Berger, E., Cowie, L. L., Kulkarni, S. R., Frail, D. A., Aussel, H., & Barger, A. J. 2003, ApJ, 588, 99

Berger, E., et al. 2000, ApJ, 545, 56

Bersier, D., et al. 2003a, ApJ, 584, L43

Bersier, D., Schild, R., & Stanek, K. Z. 2003b, GCN Circ. 2109

Bloom, J. S. 2003, in Gamma-Ray Bursts in the Afterglow Era, ed. M. Feroci et al. (San Francisco: ASP), 1

Bloom, J. S., et al. 2002, ApJ, 572, L45

Bloom, J. S., Kulkarni, S. R., & Djorgovski, S. G. 2002, AJ, 123, 1111

Boella, G., Butler, R. C., Perola, G. C., Piro, L., Scarsi, L., & Bleeker, J. A. M. 1997, A&AS, 122, 299

Burenin, R. A., et al. 2003, Astronomy Letters, 29, 573

Caldwell, N., Garnavich, P., Holland, S., Matheson, T., & Stanek, K.Z. 2003, GCN Circ. 2053

Cardelli, J. A., Clayton, G. C., & Mathis, J. S. 1989, ApJ, 345, 245

Chevalier, R. A., & Li, Z.-Y. 1999, ApJ, 520, L29

Chevalier, R. A., & Li, Z.-Y. 2000, ApJ, 536, 195

Chornock, R., Foley, R. J., Filippenko, A. V., Papenkova, M., & Weisz, D. 2003, GCN Circ. 2131

Colgate, S. A. 1968, Canadian Journal of Physics, 46, 476

Djorgovski, S. G., et al. 2001, in Gamma-ray Bursts in the Afterglow Era, ed. E. Costa, F. Frontera, & J. Hjorth (Berlin: Springer), 218

Fabricant, D., Cheimets, P., Caldwell, N., & Geary, J. 1998, PASP, 110, 79

Filippenko, A. V. 1982, PASP, 94, 715

Filippenko, A. V. 1987, ARA&A, 35, 309

Filippenko, A. V., Li, W. D., Treffers, R. R., & Modjaz, M. 2001, in Small-Telescope Astronomy on Global Scales, ed. W. P. Chen, et al. (San Francisco: ASP), 121

Foley, R. J., et al. 2003, PASP, in press (astro-ph/0307136)

Frail, D. A., Kulkarni, S. R., Berger, E., & Wieringa, M. H. 2003, AJ, 125, 2299

Fruchter, A., et al. 2003, GCN Circ. 2243

Fukugita, M., Shimasaku, K., & Ichikawa, T. 1995, PASP, 107, 945

Galama, T. J., et al. 1998a, Nature, 395, 670

Galama, T. J., et al. 1998b, ApJ, 497, L13

Garnavich, P. M., et al. 2003a, ApJ, 582, 924

Garnavich, P., et al. 2003b, IAU Circ. 8108

Garnavich, P., Matheson, T., Olszewski, E. W., Harding, P., & Stanek, K. Z. 2003c, IAU Circ. 8114

Garnavich, P. M., Stanek, K. Z., & Berlind, P. 2003d, GCN Circ. 2018

Granot, J., Nakar, E., & Piran, T. 2003, preprint (astro-ph/0304563)

Greiner, J., et al. 2003, GCN Circ. 2020

Groot, P. J., et al. 1997, IAU Circ. 6584

Hamuy, M., Walker, A. R., Suntzeff, N. B., Gigoux, P., Heathcote, S. R., & Phillips, M. M. 1992, PASP, 104, 533

Hamuy, M., Suntzeff, N. B., Heathcote, S. R., Walker, A. R., Gigoux, P., & Phillips, M. M. 1994, PASP, 106, 566

Henden, A. A. 2003, GCN Circ. 2082

Henden, A., Canzian, B., Zeh, A., & Klose, S. 2003, GCN Circ. 2110

Hjorth, J., et al. 2003, Nature, 423, 847

Hogg, D. W., & Fruchter, A. S. 1999, ApJ, 520, 54

Horne, K. 1986, PASP, 98, 609

Hunter, D. A., Hawley, W. N., & Gallagher, J. S. 1993, AJ, 106, 1797

Ibrahimov, M. A., Asfandiyarov, I. M., Kahharov, B. B., Pozanenko, A., Rumyantsev, V., Beskin, G., Zolotukhin, I., & Birykov, A. 2003, GCN Circ. 2288

Iwamoto, K., et al. 1998, Nature, 395, 672

Iwamoto, K., et al. 2000, ApJ, 534, 660

Kawabata, K. S., et al. 2003, ApJ, 593, L19

Kennicutt, R. C. 1998, ARA&A, 36, 189

Kennicutt, R. C., & Hodge, P. W. 1986, ApJ, 306, 130

Kewley, L. J., & Dopita, M. A. 2002, ApJS, 142, 35

Kinugasa, K., et al. 2002, ApJ, 577, L97

Kouveliotou, C., Meegan, C. A., Fishman, G. J., Bhat, N. P., Briggs, M. S., Koshut, T. M., Paciesas, W. S., & Pendleton, G. N. 1993, ApJ, 413, L101

Landolt, A. 1992, AJ, 104, 340

Lee, B. C., Lamb, D. Q., Tucker, D. L., & Kent, S. 2003, GCN Circ. 2096

Li, W., Chornock, R., Jha, S., & Filippenko, A. V. 2003a, GCN Circ. 2064

Li, W., Chornock, R., Jha, S., & Filippenko, A. V. 2003b, GCN Circ. 2065

Li, W., Chornock, R., Jha, S., & Filippenko, A. V. 2003c, GCN Circ. 2078

Li, W., et al. 2000, in Cosmic Explosions, ed. S. S. Holt & W. W. Zhang (New York: AIP), 103

Martini, P., Garnavich, P. M., & Stanek, K. Z. 2003, GCN Circ. 2013

Massey, P., & Gronwall, C. 1990, ApJ, 358, 344

Massey, P., Strobel, K., Barnes, J. V., & Anderson, E. 1988, ApJ, 328, 315

Matheson, T., Filippenko, A. V., Ho, L. C., Barth, A. J., & Leonard, D. C. 2000, AJ, 120, 1499

Matheson, T., et al. 2003a, GCN Circ. 2107

Matheson, T., et al. 2003b, GCN Circ. 2120

Matheson, T., et al. 2003c, ApJ, 582, L5

Mégessier, C. 1995, A&A, 296, 771

Mészáros, P. 2002, ARA&A, 40, 137

Metzger, M. R., Djorgovski, S. G., Kulkarni, S. R., Steidel, C. C., Adelberger, K. L., Frail, D. A., Costa, E., & Frontera, F. 1997, Nature, 387, 878

Miller, J. S., & Stone, R. P. S. 1993, Lick Obs. Tech. Rep., No. 66

Mulchaey, J. 2001, http://www.ociw.edu/magellan_lco/instruments/LDSS2/

Muller, G. P., Reed, R., Armandroff, T., Boroson, T. A., & Jacoby, G. H. 1998, Proc. SPIE, 3355, 577

Nakamura, T., Mazzali, P. A., Nomoto, K., & Iwamoto, K. 2001, ApJ, 550, 991

O'Donnell, J. E. 1994, ApJ, 422, 1580

Oke, J. B., et al. 1995, PASP, 107, 375

Oke, J. B., & Gunn J. E. 1983, ApJ, 266, 713

Osterbrock, D. E. 1989, Astrophysics of Gaseous Nebulae and Active Galactic Nuclei (Mill Valley: University Science Books)

Pagel, B. E. J. 1986, PASP, 98, 1009

Patat, F., & Piemonte A. 1998, IAU Circ. 6918

Patat, F., et al. 2001, ApJ, 555, 900

Pei, Y. C. 1992, ApJ, 395, L30

Persson, E., et al. 1995, http://www.lco.cl/lco/instruments/manuals/ir/C40IRC/C40IRC_manual.txt

Persson, S. E., Murphy, D. C., Krzeminski, W., Roth, M., & Rieke, M. J. 1998, AJ, 116, 2475

Peterson, B. A., & Price, P. A. 2003, GCN Circ. 1985

Phillips, M., Thompson, I., & Kunkel, B. 2002, http://www.lco.cl/magellan_lco/instruments/BC/

Price, P. A., et al. 2003, Nature, 423, 844

Richmond, M. W., et al. 1996, AJ, 111, 327

Russell, S. C., & Dopita, M. A. 1990, ApJS, 74, 93

Sari, R., Piran, T., & Halpern, J. P. 1999, ApJ, 519, L17

Schechter, P. L., Mateo, M., & Saha, A. 1993, PASP, 105, 1342

Schlegel, D. J., Finkbeiner, D. P., & Davis, M. 1998, ApJ, 500, 525

Schmidt, G., Weymann, R., & Foltz, C. 1989, PASP, 101, 713

Sheinis, A. I., Bolte, M., Epps, H. W., Kibrick, R. I., Miller, J. S., Radovan, M. V., Bigelow, B. C., & Sutin, B. M. 2002, PASP, 114, 851

Stanek, K. Z., et al. 2003a, ApJ, 591, L17

Stanek, K. Z., Latham, D. W., & Everett, M. E. 2003b, GCN Circ. 2244

Stanek, K. Z., Bersier, D., Calkins, M., Freedman, D. L., & Spahr, T. 2003c, GCN Circ. 2259

Stanek, K. Z., Martini, P., & Garnavich, P. M. 2003, GCN Circ. 2041

Stathakis, R. A., et al. 2000, MNRAS, 314, 807

Stetson, P. B. 1987, PASP, 99 191

Stetson, P. B. 1992, in ASP Conf. Ser. 25, Astrophysical Data Analysis Software and Systems I, ed. D. M. Worrall, C. Bimesderfer, & J. Barnes (San Francisco: ASP), 297

Stetson, P. B., & Harris, W. E. 1988, AJ, 96, 909

Stone, R. P. S. 1977, ApJ, 218, 767

Stritzinger, M., et al. 2002, AJ, 124, 2100

Tiengo, A., Mereghetti, S., Ghisellini, G., Rossi, E., Ghirlanda, G., & Schartel, N. 2003, A&A, in press, astro-ph/0305564

Torii, K. 2003, GCN Circ. 1986

Uemura, M., et al. 2003, Nature, 423, 843

Valdes, F. G. 2002, in Automated Data Analysis in Astronomy, ed. R. Gupta, H. P. Singh, & C. A. L. Bailer-Jones (New Delhi: Narosa Publishing House), 309

Vanderspek, R., et al. 2003, GCN Circ. 1997

Van Dyk, S. D., Hamuy, M., & Filippenko, A. V. 1996, AJ, 111, 2017

van Paradijs, J., Kouveliotou, C., & Wijers, R. A. M. J. 2000, ARA&A, 38, 379

van Paradijs, J., et al. 1997, Nature, 386, 686

Wade, R. A., & Horne, K. D. 1988, ApJ, 324, 411

Weymann, R., Kunkel, B., McWilliam, A., & Phillips, M. 1999, http://www.ociw.edu/lco/instruments/manuals/wfccd/wfccd_manual.html

Woosley, S. E. 1993, ApJ, 405, 273

Woosley, S. E., Eastman, R. G., & Schmidt, B. P. 1999, ApJ, 516, 788

Woosley, S. E., & MacFadyen, A. I. 1999, A&AS, 138, 499

Zeh, A., Klose, S. & Greiner, J. 2003, GCN Circ. 2081

This preprint was prepared with the AAS LaTeX macros v5.0.

Table 1. JOURNAL OF PHOTOMETRIC OBSERVATIONS

ΔT[a]	Mag	σ_m	Filter	Observatory[b]
0.6494	15.296	0.020	U	FLWO
0.6601	15.346	0.020	U	FLWO
0.6796	15.394	0.050	U	KAIT
0.6841	15.381	0.020	U	FLWO
0.6989	15.369	0.010	U	FLWO
0.7041	15.442	0.040	U	KAIT
0.7091	15.434	0.010	U	FLWO
0.7191	15.490	0.010	U	FLWO
0.7198	15.458	0.050	U	KAIT
0.7291	15.525	0.010	U	FLWO
0.7391	15.557	0.010	U	FLWO
0.7505	15.584	0.010	U	FLWO
0.7590	15.599	0.050	U	KAIT
0.7609	15.610	0.010	U	FLWO
0.7712	15.630	0.010	U	FLWO
0.7746	15.624	0.040	U	KAIT
0.7816	15.643	0.010	U	FLWO
0.7920	15.678	0.010	U	FLWO
0.8023	15.715	0.010	U	FLWO
0.8098	15.707	0.050	U	KAIT
0.8127	15.758	0.020	U	FLWO
0.8231	15.774	0.020	U	FLWO
0.8324	15.814	0.050	U	KAIT
0.8334	15.823	0.020	U	FLWO
0.8438	15.775	0.020	U	FLWO
0.8536	15.851	0.060	U	KAIT
0.8542	15.850	0.020	U	FLWO
0.8645	15.862	0.020	U	FLWO
0.8694	15.993	0.060	U	KAIT
0.8749	15.941	0.020	U	FLWO
0.8853	15.936	0.060	U	KAIT
0.8853	15.963	0.020	U	FLWO
0.8956	15.982	0.020	U	FLWO

Table 1—Continued

ΔT[a]	Mag	σ_m	Filter	Observatory[b]
0.9039	16.025	0.060	U	KAIT
0.9059	16.059	0.020	U	FLWO
0.9164	16.063	0.020	U	FLWO
0.9199	16.086	0.070	U	KAIT
0.9268	16.072	0.020	U	FLWO
0.9360	16.087	0.080	U	KAIT
0.9371	16.118	0.020	U	FLWO
0.9475	16.155	0.030	U	FLWO
0.9578	16.176	0.030	U	FLWO
1.6398	16.415	0.020	U	FLWO
1.7351	16.539	0.020	U	FLWO
1.7852	16.546	0.060	U	KAIT
1.8337	16.681	0.020	U	FLWO
1.9092	16.771	0.020	U	FLWO
2.8438	17.282	0.020	U	FLWO
2.9549	17.329	0.030	U	FLWO
3.7822	17.578	0.030	U	FLWO
3.8012	17.610	0.030	U	FLWO
3.8262	17.670	0.030	U	FLWO
3.8454	17.704	0.030	U	FLWO
4.6574	18.060	0.030	U	FLWO
5.6493	18.011	0.040	U	FLWO
6.6648	18.664	0.060	U	FLWO
0.6411	15.903	0.010	B	FLWO
0.6518	15.921	0.010	B	FLWO
0.6663	15.977	0.010	B	FLWO
0.6836	16.013	0.020	B	KAIT
0.6863	16.033	0.010	B	FLWO
0.6912	16.036	0.010	B	FLWO
0.7019	16.085	0.010	B	FLWO
0.7080	16.076	0.020	B	KAIT
0.7120	16.100	0.010	B	FLWO
0.7220	16.146	0.010	B	FLWO

Table 1—Continued

ΔT^{a}	Mag	σ_m	Filter	Observatory[b]
0.7238	16.117	0.010	B	KAIT
0.7320	16.185	0.010	B	FLWO
0.7432	16.161	0.010	B	FLWO
0.7536	16.212	0.010	B	FLWO
0.7629	16.229	0.010	B	KAIT
0.7639	16.242	0.010	B	FLWO
0.7743	16.286	0.010	B	FLWO
0.7786	16.288	0.020	B	KAIT
0.7847	16.302	0.010	B	FLWO
0.7950	16.328	0.010	B	FLWO
0.8054	16.346	0.010	B	FLWO
0.8138	16.374	0.030	B	KAIT
0.8157	16.379	0.010	B	FLWO
0.8262	16.386	0.010	B	FLWO
0.8363	16.400	0.030	B	KAIT
0.8365	16.429	0.010	B	FLWO
0.8468	16.444	0.010	B	FLWO
0.8572	16.491	0.010	B	FLWO
0.8576	16.505	0.040	B	KAIT
0.8676	16.519	0.010	B	FLWO
0.8734	16.505	0.030	B	KAIT
0.8780	16.542	0.010	B	FLWO
0.8883	16.562	0.020	B	FLWO
0.8893	16.531	0.050	B	KAIT
0.8986	16.626	0.020	B	FLWO
0.9079	16.595	0.070	B	KAIT
0.9090	16.640	0.020	B	FLWO
0.9195	16.654	0.020	B	FLWO
0.9239	16.676	0.030	B	KAIT
0.9298	16.665	0.020	B	FLWO
0.9399	16.710	0.020	B	KAIT
0.9402	16.724	0.020	B	FLWO
0.9505	16.748	0.020	B	FLWO

Table 1—Continued

ΔT^{a}	Mag	σ_m	Filter	Observatory[b]
1.6447	17.002	0.010	B	FLWO
1.7399	17.132	0.010	B	FLWO
1.7909	17.210	0.020	B	KAIT
1.8385	17.267	0.010	B	FLWO
1.9144	17.331	0.010	B	FLWO
2.8485	17.805	0.020	B	FLWO
2.9596	17.937	0.020	B	FLWO
3.7261	18.104	0.040	B	FLWO
3.7875	18.154	0.020	B	FLWO
3.8125	18.197	0.020	B	FLWO
3.8316	18.221	0.020	B	FLWO
3.8621	18.244	0.020	B	FLWO
4.6437	18.632	0.020	B	FLWO
5.6356	18.528	0.030	B	FLWO
5.7063	18.548	0.040	B	LCO100
5.7100	18.569	0.040	B	LCO100
6.5796	19.076	0.040	B	LCO100
6.5840	19.069	0.040	B	LCO100
6.6511	19.053	0.030	B	FLWO
6.8690	19.149	0.030	B	FLWO
7.6383	19.478	0.060	B	FLWO
7.8741	19.632	0.050	B	FLWO
8.6528	19.699	0.060	B	FLWO
8.7897	19.774	0.040	B	FLWO
8.8919	19.698	0.040	B	FLWO
9.6497	19.750	0.050	B	FLWO
9.7762	19.871	0.040	B	FLWO
9.8720	19.820	0.060	B	FLWO
10.7558	19.953	0.040	B	FLWO
11.7358	20.112	0.040	B	FLWO
12.7403	20.394	0.050	B	FLWO
21.7000	21.296	0.060	B	FLWO
22.6667	21.241	0.070	B	FLWO

Table 1—Continued

ΔT[a]	Mag	σ_m	Filter	Observatory[b]
23.6814	21.382	0.070	B	FLWO
24.6858	21.440	0.060	B	FLWO
25.6888	21.671	0.040	B	KPNO4m
25.6968	21.583	0.040	B	KPNO4m
25.7402	21.516	0.060	B	FLWO
26.6888	21.675	0.040	B	KPNO4m
26.6968	21.660	0.040	B	KPNO4m
26.7191	21.644	0.080	B	FLWO
27.6718	21.714	0.030	B	KPNO4m
27.6878	21.725	0.020	B	KPNO4m
28.6688	21.794	0.030	B	KPNO4m
29.6408	21.869	0.060	B	KPNO4m
29.6528	21.900	0.020	B	KPNO4m
30.6808	21.971	0.030	B	KPNO4m
31.6678	22.034	0.020	B	KPNO4m
31.6748	22.023	0.020	B	KPNO4m
32.6818	22.066	0.040	B	KPNO4m
33.6558	22.124	0.030	B	KPNO4m
33.6628	22.173	0.050	B	KPNO4m
34.6538	22.121	0.050	B	KPNO4m
34.6608	22.185	0.040	B	KPNO4m
36.5578	22.268	0.040	B	LCO100
37.5148	22.285	0.040	B	LCO100
37.6718	22.254	0.040	B	KPNO4m
37.6808	22.357	0.040	B	KPNO4m
38.5538	22.273	0.040	B	LCO100
39.5468	22.335	0.060	B	LCO100
0.6432	15.545	0.010	V	FLWO
0.6539	15.574	0.010	V	FLWO
0.6709	15.614	0.010	V	FLWO
0.6876	15.729	0.030	V	KAIT
0.6927	15.692	0.010	V	FLWO
0.7036	15.720	0.010	V	FLWO

Table 1—Continued

ΔT^a	Mag	σ_m	Filter	Observatory[b]
0.7111	15.770	0.010	V	KAIT
0.7136	15.750	0.010	V	FLWO
0.7236	15.784	0.010	V	FLWO
0.7269	15.807	0.010	V	KAIT
0.7336	15.809	0.010	V	FLWO
0.7450	15.822	0.010	V	FLWO
0.7554	15.851	0.010	V	FLWO
0.7657	15.893	0.010	V	FLWO
0.7660	15.931	0.030	V	KAIT
0.7761	15.911	0.010	V	FLWO
0.7817	15.965	0.030	V	KAIT
0.7865	15.946	0.010	V	FLWO
0.7968	15.962	0.010	V	FLWO
0.8072	15.977	0.010	V	FLWO
0.8176	16.034	0.010	V	FLWO
0.8178	16.070	0.020	V	KAIT
0.8280	16.051	0.010	V	FLWO
0.8383	16.069	0.010	V	FLWO
0.8395	16.139	0.020	V	KAIT
0.8486	16.104	0.010	V	FLWO
0.8590	16.155	0.010	V	FLWO
0.8607	16.192	0.020	V	KAIT
0.8694	16.151	0.010	V	FLWO
0.8765	16.239	0.030	V	KAIT
0.8798	16.194	0.010	V	FLWO
0.8901	16.208	0.020	V	FLWO
0.8924	16.254	0.050	V	KAIT
0.9004	16.247	0.020	V	FLWO
0.9109	16.245	0.020	V	FLWO
0.9110	16.269	0.070	V	KAIT
0.9213	16.309	0.020	V	FLWO
0.9270	16.360	0.050	V	KAIT
0.9316	16.331	0.020	V	FLWO

Table 1—Continued

ΔT^a	Mag	σ_m	Filter	Observatory[b]
0.9420	16.336	0.020	V	FLWO
0.9432	16.395	0.040	V	KAIT
0.9523	16.366	0.020	V	FLWO
1.6482	16.628	0.010	V	FLWO
1.7435	16.737	0.010	V	FLWO
1.7949	16.861	0.030	V	KAIT
1.8421	16.859	0.010	V	FLWO
1.8564	16.906	0.070	V	KAIT
1.9179	16.925	0.010	V	FLWO
2.8520	17.416	0.010	V	FLWO
2.9632	17.486	0.020	V	FLWO
3.7296	17.717	0.050	V	FLWO
3.7720	17.748	0.020	V	FLWO
3.7911	17.757	0.020	V	FLWO
3.8160	17.783	0.020	V	FLWO
3.8352	17.825	0.020	V	FLWO
3.8657	17.814	0.020	V	FLWO
4.6472	18.110	0.020	V	FLWO
5.6391	18.110	0.020	V	FLWO
5.7150	18.099	0.020	V	LCO100
5.7177	18.072	0.020	V	LCO100
6.5882	18.585	0.020	V	LCO100
6.5908	18.584	0.020	V	LCO100
6.6546	18.617	0.020	V	FLWO
6.8737	18.716	0.020	V	FLWO
7.6431	19.064	0.040	V	FLWO
7.8788	19.024	0.040	V	FLWO
8.6401	19.158	0.060	V	FLWO
8.7770	19.225	0.040	V	FLWO
8.8792	19.227	0.040	V	FLWO
9.6370	19.170	0.060	V	FLWO
9.7635	19.206	0.030	V	FLWO
9.8592	19.194	0.050	V	FLWO

Table 1—Continued

ΔT^a	Mag	σ_m	Filter	Observatory[b]
10.6658	19.452	0.050	V	FLWO
10.8158	19.458	0.040	V	FLWO
11.6590	19.575	0.040	V	FLWO
11.7723	19.570	0.040	V	FLWO
25.6828	20.632	0.040	V	KPNO4m
25.7038	20.620	0.030	V	KPNO4m
26.6778	20.701	0.040	V	KPNO4m
26.6838	20.680	0.040	V	KPNO4m
27.6668	20.812	0.020	V	KPNO4m
27.6828	20.815	0.020	V	KPNO4m
28.6748	20.885	0.020	V	KPNO4m
29.6358	20.953	0.040	V	KPNO4m
29.6468	20.948	0.020	V	KPNO4m
30.6878	21.058	0.020	V	KPNO4m
31.6558	21.080	0.020	V	KPNO4m
31.6618	21.090	0.020	V	KPNO4m
32.6888	21.122	0.030	V	KPNO4m
33.6428	21.210	0.030	V	KPNO4m
33.6488	21.224	0.020	V	KPNO4m
33.6818	21.160	0.040	V	KPNO4m
34.6468	21.337	0.050	V	KPNO4m
34.6698	21.310	0.050	V	KPNO4m
36.5368	21.374	0.030	V	LCO100
36.6688	21.392	0.030	V	KPNO4m
36.6768	21.360	0.030	V	KPNO4m
37.4928	21.433	0.030	V	LCO100
38.5468	21.487	0.030	V	LCO100
39.5328	21.468	0.030	V	LCO100
0.5678	15.021	0.020	R	Clay
0.5698	14.990	0.020	R	Clay
0.6251	15.182	0.010	R	FLWO
0.6276	15.165	0.010	R	FLWO
0.6307	15.180	0.010	R	FLWO

Table 1—Continued

ΔT[a]	Mag	σ_m	Filter	Observatory[b]
0.6452	15.228	0.010	R	FLWO
0.6559	15.266	0.010	R	FLWO
0.6755	15.306	0.010	R	FLWO
0.6920	15.400	0.030	R	KAIT
0.6943	15.381	0.010	R	FLWO
0.7049	15.387	0.010	R	FLWO
0.7133	15.424	0.020	R	KAIT
0.7150	15.422	0.010	R	FLWO
0.7250	15.464	0.010	R	FLWO
0.7291	15.463	0.010	R	KAIT
0.7350	15.502	0.010	R	FLWO
0.7464	15.504	0.010	R	FLWO
0.7567	15.535	0.010	R	FLWO
0.7671	15.576	0.010	R	FLWO
0.7683	15.594	0.020	R	KAIT
0.7775	15.578	0.010	R	FLWO
0.7839	15.635	0.020	R	KAIT
0.7878	15.624	0.010	R	FLWO
0.7982	15.634	0.010	R	FLWO
0.8086	15.664	0.010	R	FLWO
0.8190	15.702	0.010	R	FLWO
0.8218	15.700	0.010	R	KAIT
0.8293	15.750	0.010	R	FLWO
0.8396	15.742	0.010	R	FLWO
0.8417	15.785	0.080	R	KAIT
0.8500	15.774	0.010	R	FLWO
0.8604	15.802	0.010	R	FLWO
0.8630	15.801	0.010	R	KAIT
0.8708	15.852	0.010	R	FLWO
0.8787	15.875	0.010	R	KAIT
0.8811	15.875	0.010	R	FLWO
0.8915	15.885	0.010	R	FLWO
0.8947	15.883	0.020	R	KAIT

Table 1—Continued

ΔT^a	Mag	σ_m	Filter	Observatory[b]
0.9018	15.909	0.010	R	FLWO
0.9123	15.946	0.010	R	FLWO
0.9132	15.924	0.020	R	KAIT
0.9226	15.983	0.020	R	FLWO
0.9293	15.941	0.020	R	KAIT
0.9330	16.002	0.020	R	FLWO
0.9433	16.034	0.020	R	FLWO
0.9454	16.078	0.060	R	KAIT
0.9537	16.069	0.020	R	FLWO
1.5838	16.233	0.020	R	Clay
1.5848	16.230	0.020	R	Clay
1.5858	16.225	0.020	R	Clay
1.5868	16.227	0.020	R	Clay
1.6514	16.271	0.010	R	FLWO
1.7466	16.403	0.010	R	FLWO
1.7989	16.536	0.020	R	KAIT
1.8452	16.541	0.010	R	FLWO
1.8611	16.647	0.070	R	KAIT
1.9211	16.575	0.010	R	FLWO
2.5778	16.815	0.020	R	Clay
2.5788	16.849	0.020	R	Clay
2.5808	16.858	0.020	R	Clay
2.5818	16.856	0.020	R	Clay
2.8552	17.069	0.010	R	FLWO
2.9663	17.152	0.010	R	FLWO
3.5868	17.241	0.020	R	Clay
3.5968	17.245	0.020	R	Clay
3.5978	17.254	0.020	R	Clay
3.5988	17.242	0.020	R	Clay
3.5998	17.252	0.020	R	Clay
3.6058	17.230	0.020	R	Clay
3.7328	17.361	0.030	R	FLWO
3.7752	17.387	0.020	R	FLWO

Table 1—Continued

ΔT^{a}	Mag	σ_m	Filter	Observatory[b]
3.7942	17.408	0.010	R	FLWO
3.8192	17.433	0.010	R	FLWO
3.8383	17.462	0.010	R	FLWO
3.8688	17.491	0.020	R	FLWO
4.6008	17.799	0.020	R	Clay
4.6048	17.788	0.020	R	Clay
4.6058	17.788	0.020	R	Clay
4.6068	17.795	0.020	R	Clay
4.6088	17.797	0.020	R	Clay
4.6098	17.803	0.020	R	Clay
4.6348	17.807	0.020	R	Clay
4.6368	17.803	0.020	R	Clay
4.6388	17.826	0.020	R	Clay
4.6504	17.790	0.020	R	FLWO
5.6423	17.776	0.020	R	FLWO
6.6578	18.253	0.020	R	FLWO
6.8776	18.395	0.020	R	FLWO
7.6469	18.734	0.030	R	FLWO
7.8827	18.750	0.040	R	FLWO
8.6440	18.848	0.030	R	FLWO
8.6653	18.834	0.040	R	FLWO
8.7808	18.845	0.030	R	FLWO
8.8830	18.881	0.030	R	FLWO
9.6409	18.891	0.030	R	FLWO
9.7674	18.935	0.030	R	FLWO
9.8631	18.942	0.040	R	FLWO
10.6708	19.097	0.040	R	FLWO
10.8258	19.050	0.030	R	FLWO
11.6529	19.246	0.030	R	FLWO
11.6940	19.209	0.030	R	FLWO
11.8158	19.258	0.030	R	FLWO
12.6858	19.305	0.030	R	FLWO
12.8158	19.358	0.040	R	FLWO

Table 1—Continued

ΔT[a]	Mag	σ_m	Filter	Observatory[b]
13.6344	19.414	0.080	R	FLWO
13.6590	19.480	0.080	R	FLWO
19.6958	19.777	0.040	R	FLWO
19.7354	19.807	0.040	R	FLWO
19.7822	19.815	0.060	R	FLWO
20.7058	19.859	0.040	R	FLWO
20.8038	19.937	0.050	R	FLWO
20.8398	19.795	0.050	R	FLWO
21.6588	19.938	0.030	R	FLWO
21.7862	19.949	0.040	R	FLWO
21.8729	19.866	0.060	R	FLWO
22.6098	19.945	0.050	R	LCO40
22.6448	20.017	0.040	R	FLWO
22.7344	20.006	0.040	R	FLWO
23.6582	20.080	0.030	R	FLWO
23.7544	20.043	0.040	R	FLWO
24.6514	20.146	0.040	R	FLWO
24.8058	20.117	0.030	R	FLWO
25.6658	20.158	0.020	R	KPNO4m
25.7001	20.142	0.040	R	FLWO
25.7098	20.148	0.020	R	KPNO4m
25.7178	20.175	0.040	R	FLWO
26.6718	20.255	0.040	R	FLWO
27.7108	20.320	0.050	R	FLWO
28.7200	20.229	0.050	R	FLWO
28.7314	20.347	0.060	R	FLWO
29.6629	20.422	0.040	R	FLWO
29.6781	20.350	0.040	R	FLWO
29.6895	20.422	0.050	R	FLWO
30.6941	20.478	0.040	R	FLWO
30.7201	20.493	0.040	R	FLWO
31.7105	20.568	0.040	R	FLWO
32.5908	20.549	0.070	R	LCO40

Table 1—Continued

ΔT[a]	Mag	σ_m	Filter	Observatory[b]
32.6581	20.588	0.040	R	FLWO
33.6338	20.665	0.030	R	KPNO4m
33.8010	20.563	0.060	R	FLWO
33.8173	20.657	0.060	R	FLWO
34.5648	20.700	0.040	R	KPNO4m
34.6919	20.812	0.070	R	FLWO
34.7081	20.705	0.050	R	FLWO
36.8058	20.875	0.080	R	FLWO
37.6631	20.820	0.070	R	FLWO
37.6738	20.897	0.050	R	FLWO
37.6846	20.823	0.060	R	FLWO
38.7300	21.024	0.060	R	FLWO
39.6716	21.012	0.070	R	FLWO
51.7458	21.553	0.060	R	FLWO
52.7058	21.698	0.110	R	FLWO
53.7408	21.430	0.080	R	FLWO
54.6944	21.309	0.090	R	FLWO
57.7163	21.612	0.060	R	FLWO
59.7069	21.456	0.070	R	FLWO
60.7058	21.618	0.090	R	FLWO
0.6470	14.820	0.010	I	FLWO
0.6577	14.845	0.010	I	FLWO
0.6801	14.896	0.010	I	FLWO
0.6959	14.937	0.010	I	FLWO
0.6961	14.974	0.030	I	KAIT
0.7062	14.981	0.010	I	FLWO
0.7155	14.995	0.030	I	KAIT
0.7162	15.045	0.010	I	FLWO
0.7262	15.053	0.010	I	FLWO
0.7313	15.034	0.020	I	KAIT
0.7362	15.042	0.010	I	FLWO
0.7477	15.103	0.010	I	FLWO
0.7580	15.134	0.010	I	FLWO

Table 1—Continued

ΔT^a	Mag	σ_m	Filter	Observatory[b]
0.7684	15.173	0.010	I	FLWO
0.7705	15.133	0.030	I	KAIT
0.7788	15.182	0.010	I	FLWO
0.7862	15.219	0.030	I	KAIT
0.7891	15.225	0.010	I	FLWO
0.7995	15.218	0.020	I	FLWO
0.8098	15.232	0.020	I	FLWO
0.8203	15.287	0.010	I	FLWO
0.8259	15.286	0.020	I	KAIT
0.8306	15.331	0.010	I	FLWO
0.8409	15.352	0.020	I	FLWO
0.8440	15.300	0.030	I	KAIT
0.8513	15.380	0.010	I	FLWO
0.8616	15.420	0.020	I	FLWO
0.8652	15.402	0.020	I	KAIT
0.8721	15.411	0.020	I	FLWO
0.8810	15.424	0.020	I	KAIT
0.8824	15.407	0.020	I	FLWO
0.8927	15.424	0.020	I	FLWO
0.8969	15.471	0.020	I	KAIT
0.9031	15.443	0.020	I	FLWO
0.9136	15.511	0.020	I	FLWO
0.9155	15.534	0.020	I	KAIT
0.9239	15.606	0.020	I	FLWO
0.9316	15.571	0.040	I	KAIT
0.9343	15.648	0.020	I	FLWO
0.9446	15.648	0.020	I	FLWO
0.9477	15.569	0.030	I	KAIT
0.9550	15.649	0.030	I	FLWO
1.6542	15.828	0.010	I	FLWO
1.7495	15.950	0.010	I	FLWO
1.8029	16.044	0.040	I	KAIT
1.8481	16.087	0.010	I	FLWO

Table 1—Continued

ΔT[a]	Mag	σ_m	Filter	Observatory[b]
1.8652	16.059	0.070	I	KAIT
1.9239	16.123	0.010	I	FLWO
2.8581	16.594	0.010	I	FLWO
2.9692	16.681	0.020	I	FLWO
3.7780	16.957	0.020	I	FLWO
3.7970	16.979	0.020	I	FLWO
3.8220	16.971	0.020	I	FLWO
3.8412	17.014	0.020	I	FLWO
3.8717	17.027	0.050	I	FLWO
4.6532	17.363	0.020	I	FLWO
5.6451	17.319	0.020	I	FLWO
5.7205	17.369	0.020	I	LCO100
5.7224	17.365	0.020	I	LCO100
6.5936	17.830	0.020	I	LCO100
6.5956	17.878	0.030	I	LCO100
6.6606	17.899	0.030	I	FLWO
6.8811	17.968	0.030	I	FLWO
7.6504	18.315	0.040	I	FLWO
7.8862	18.386	0.050	I	FLWO
8.6475	18.473	0.040	I	FLWO
8.7844	18.469	0.040	I	FLWO
8.8866	18.518	0.050	I	FLWO
9.6444	18.595	0.050	I	FLWO
9.7709	18.527	0.040	I	FLWO
9.8666	18.583	0.060	I	FLWO
10.6807	18.741	0.050	I	FLWO
10.8158	18.768	0.040	I	FLWO
11.6667	18.906	0.040	I	FLWO
11.7475	18.938	0.050	I	FLWO
11.8441	18.985	0.060	I	FLWO
3.6058	15.935	0.020	J	LCO40
4.6488	16.449	0.030	J	LCO40
5.6552	16.416	0.020	J	LCO40

Table 1—Continued

ΔT[a]	Mag	σ_m	Filter	Observatory[b]
6.6239	17.051	0.040	J	LCO40
7.6887	17.438	0.030	J	LCO40
8.6377	17.559	0.040	J	LCO40
9.6427	17.736	0.040	J	LCO40
11.6355	18.233	0.070	J	LCO40
3.6325	15.222	0.020	H	LCO40
4.6757	15.575	0.030	H	LCO40
5.6775	15.687	0.030	H	LCO40
6.6493	16.199	0.040	H	LCO40
7.6682	16.634	0.050	H	LCO40
8.6645	16.833	0.080	H	LCO40
9.6795	17.152	0.050	H	LCO40

Note. — [The complete version of this table is in the electronic edition of the Journal. The printed edition contains only a sample.]

[a]Days after 2003 March 29.4842 UT.

[b] FLWO: F. L. Whipple Observatory 1.2-m telescope; KAIT: 0.76-m Katzman Automatic Imaging Telescope; LCO100: Las Campanas Observatory 2.5-m telescope (du Pont); KPNO4m: Kitt Peak National Observatory 4-m telescope; Clay: Magellan Clay telescope; LCO40: Las Campanas Observatory 1-m telescope (Swope)

Table 2. JOURNAL OF SPECTROSCOPIC OBSERVATIONS

ΔT[a]	UT Date[b]	Julian Day[b]	Tel.[c]	Range[d] (Å)	Res.[e] (Å)	P.A.[f] (°)	Par.[g] (°)	Air.[h]	Flux Std.[i]	See.[j] (″)	Slit (″)	Exp. (s)
0.72	2003-03-30.20	2452728.70	FLWO	3720-7540	6.4	0.0	-40.2	1.03	F34	2	3.0	2×1200
0.75	2003-03-30.23	2452728.73	MMT	3600-8700	8.0	-16	-4.9	1.02	CygOB2/H600	4.5	1.25	4×900
1.73	2003-03-31.21	2452729.71	MMT	3600-8700	8.0	-43	-26.8	1.03	CygOB2/H600	1.5	1.25	3×600
2.66	2003-04-01.14	2452730.64	MMT	3450-8650	6.4	-65	-54.1	1.18	F34/H600	1.5	1.0	900
2.75	2003-04-01.23	2452730.73	FLWO	3720-7540	6.4	5.0	7.9	1.02	F34	2	3.0	1200
3.70	2003-04-02.18	2452731.68	MMT	3450-8650	6.4	-52	-40.6	1.06	F34/HD84	2.5	1.0	4×600
3.82	2003-04-02.30	2452731.80	FLWO	3720-7540	6.4	53	62.2	1.13	F34	2	3.0	2×1800
4.66	2003-04-03.14	2452732.64	MMT	3450-8600	6.4	-64	-52.5	1.15	F34/HD84	2.5	1.0	900
5.72	2003-04-04.22	2452733.72	D25	3800-9320	7.7	A.P.[k]	-40	2.16	L3218/L7379/L7987	···	1.6	2×600
5.80	2003-04-04.28	2452733.78	MMT	3450-8600	8.0	52	41.6	1.06	F34/HD84	2	1.5	900
6.60	2003-04-05.10	2452734.60	D25	3800-9320	7.7	A.P.[k]	-9	1.59	L7379/L7987	···	1.6	900
6.66	2003-04-05.14	2452734.64	MMT	3500-8650	6.4	-62	-61.0	1.11	F34/HD84	2	1.0	2×900
7.67	2003-04-06.15	2452735.65	MMT	3500-8650	6.4	-61	-45.6	1.08	F34/HD84	2.5	1.0	2×1200
8.78	2003-04-07.26	2452736.76	MMT	3300-8450	8.0	48	50.8	1.05	F34/HD84	3	1.25	3×900
9.63	2003-04-08.13	2452737.63	D25	3800-9320	7.7	A.P.[k]	6	1.58	L7379/L7987	···	1.6	2×900
9.67	2003-04-08.15	2452737.65	MMT	3250-8300	6.4	-61	-57.2	1.07	F34/HD84	3	1.0	3×900
9.86	2003-04-08.34	2452737.84	L3	3176-10400	6-15	188	54	1.21	F34/HD84	3.5	2	4×2400
10.68	2003-04-09.16	2452738.66	MMT	3200-8350	8.0	-60	-45.0	1.08	F34/HD84	3.5	1.25	3×1200
11.66	2003-04-10.16	2452739.66	Clay	3600-9000	10.4	A.P.[k]	-28	1.65	F67/L3218	···	0.7	2×900
11.66	2003-04-10.14	2452739.64	MMT	3200-8350	8.0	-62	-49.2	1.11	F34/HD84	3.0	1.25	3×900
25.71	2003-04-24.19	2452753.69	MMT	3700-8100	6.4	10	13.6	1.02	F34/HD84	1.5	1.0	3×1800
25.89	2003-04-24.37	2452753.87	KII	4110-9154	2.0	-99	88.62	1.1	F34	1.4	1.25	3×600
33.57	2003-05-02.05	2452761.55	Baade	3400-8002	10.5	182	-11.5	1.61	F66/HD84	1.2	1.0	4×1800
35.53	2003-05-04.01	2452763.51	Baade	3400-8002	10.5	178	2.0	1.57	F66/HD84	1.5	1.0	4×1800

Table 2—Continued

ΔT[a]	UT Date[b]	Julian Day[b]	Tel.[c]	Range[d] (Å)	Res.[e] (Å)	P.A.[f] (°)	Par.[g] (°)	Air.[h]	Flux Std.[i]	See.[j] (″)	Slit (″)	Exp. (s)
36.55	2003-05-05.03	2452764.53	Baade	6240-9220	5.1	179	180	1.57	HD84	1.5	1.0	4×1800
55.90	2003-05-24.38	2452783.38	KI	3260-9280	8.0	79.9	79.4	1.80	BD28/BD17	1.3	1.5	3×900

Note. — Not all spectra listed in this Table are shown in the paper.

[a]Days since 2003 March 29.4842 UT.

[b]Midpoint of observation(s).

[c]MMT = MMT 6.5m/Blue Channel; FLWO = FLWO 1.5m/FAST; D25 = du Pont 2.5m/WFCCD; L3 = Lick 3m/Kast; Clay = Magellan 6.5m Clay/LDSS2; KII = Keck II 10m/ESI; Baade = Magellan 6.5m Baade/Boller & Chivens; KI = Keck I 10m/LRIS.

[d]Observed wavelength range of spectrum. In some cases, the extreme ends are noisy, and are not shown in the figures.

[e]Approximate spectral resolution (full width at half maximum intensity), typically estimated from night-sky emission lines.

[f]Approximate average position angle of the spectrograph slit.

[g]Optimal parallactic angle over the course of the exposures.

[h]Average airmass of observations.

[i]The standard stars are as follows: BD28 = BD+28°4211, F34 = Feige 34, H600 = Hiltner 600—Stone (1977), Massey & Gronwall (1990); F66 = Feige 66, F67 = Feige 67, CygOB2 = Cyg OB2 No. 9—Massey et al. (1988); HD84 = HD 84937, BD17 = BD+47°4708—Oke & Gunn (1983); L3218 = LTT 3218, L7379 = LTT 7379, L7987 = LTT 7987—Hamuy et al. (1992; 1994).

[j]Approximate seeing, estimated from the data and observers' records.

[k]A.P. = At Parallactic.

Table 3. EMISSION LINE RATIOS

log ([O III] $\lambda5007$/[O II] $\lambda3727$)	log ([N II] $\lambda6584$/[O II] $\lambda3727$)	log ([O II]+[O III])/Hβ	log ([N II] $\lambda6584$/Hα)	Hα/Hβ	Hγ/Hβ	log ([N II] $\lambda6584$/[O III] $\lambda5007$)
0.2	< -0.9	0.9	< -1.0	3.0	0.4	< -1.3

Table 4. GRB/SN FITS

ΔT[a]	Best SN[b]	SN %[c]	Fit Range (Å)[d]	Fit Error[e]	SN % B[f]	SN % R[f]
0.75	SN 1997ef +44	5	4242-8000	0.025	2	6
1.73	SN 1997ef +44	5	4242-8000	0.025	2	6
2.66	SN 1997ef +84	2	4348-8000	0.087	1	3
3.70	SN 2002ap +28	2	4348-8000	0.570	1	2
4.66	SN 1997ef +25	6	4236-8000	0.134	2	7
5.80	SN 1997ef -11	1	4348-8000	0.056	1	1
6.66	SN 1998bw +11	8	3950-8000	0.110	4	10
7.67	SN 2002ap +6	6	4348-8000	0.853	3	8
8.78	SN 1998bw -7	13	3906-8000	0.459	11	15
9.67	SN 1998bw -6	26	3920-8000	0.135	21	30
10.68	SN 1997ef -11	19	4348-8000	2.949	14	22
11.66	SN 1998bw -3	38	4092-8000	1.067	29	43
25.80	SN 1998bw +6	61	3950-8000	0.695	46	68
33.57	SN 1998bw +13	63	3622-8000	2.154	45	72
35.53	SN 1998bw +11	86	3950-8000	3.921	76	89

[a]Days since 2003 March 29.4842 UT.

[b]SN spectrum that best matches the OT afterglow at this epoch (SN and approximate phase relative to B-band maximum). Note that the low SN fraction at early times ($\Delta T = 0.75 - 7.67$ days) makes the SN spectrum listed almost arbitrary.

[c]Percentage of SN component in best-fit spectrum over the fitting range listed.

[d]Spectral range of the overall fit.

[e]Least-squares deviation from fit (not a formal χ^2 statistic). Only the relative size of this number is important.

[f]Relative contribution of the SN in the broad-band filter indicated, synthesized from the best-fit, scaled SN spectrum.